Growth and Transport Properties of [Rare Earth]TiO3/SrTiO3 Interfaces

Lebedev, N.

6

On a possible Kondo effect in $LaAlO_3/Eu_{1-x}La_xTiO_3/SrTiO_3$ heterostructures

In this chapter, we study $LaAlO_3/Eu_{1-x}La_xTiO_3/SrTiO_3$ structures with different thicknesses of the $Eu_{1-x}La_xTiO_3$ layer and for x = 0 ($EuTiO_3$) and x = 0.1. We observe that both systems have many properties similar to previously studied $LaAlO_3/EuTiO_3/SrTiO_3$ and other oxide interfaces, such as the formation of a 2D electron gas for 1 or 2 unit cells of $Eu_{1-x}La_xTiO_3$, a metal-insulator transition driven by the thickness increase of $Eu_{1-x}La_xTiO_3$ layer, the presence of an Anomalous Hall effect (AHE) when driving the systems above the Lifshitz point with a backgate voltage, and a minimum in the temperature dependence of the sheet resistance below the Lifshitz point in the one-band regime. However, and notwithstanding the likely presence of magnetism in the system, we do not attribute that minimum to the Kondo effect, but rather to the properties of $SrTiO_3$ crystal and the inevitable effects of charge trapping when using back gates.

6.1. Introduction

Oxide interfaces, mainly based on the $SrTiO_3$ (STO), are systems that have significant freedom of manipulating various properties by applying a gate voltage. Among them, tunable spin polarisation or magnetism, and its signature, the Anomalous Hall effect (AHE), have been extensively studied in the past decade in various STO-based structures [78, 91, 96, 132, 133, 135] (also Chapter 3). The AHE can be completely switched off by a gate voltage. The switch point is strongly connected to the so-called Lifshitz transition [36], which separates two regimes with only $3d_{xy}$ type of orbitals occupied, leading to single band transport, and with $3d_{xy}$ and $3d_{xz/yz}$ and the involvement of two bands. The latter regime coincides with the presence of AHE and, therefore, spin-polarisation [36, 91, 96, 132, 133, 135], whereas the former one a non-spin polarised state where, however, a non-monotonous temperature dependence of resistance with a pronounced minimum has been observed. This behavior of the sheet resistance has been attributed to the Kondo-regime [132, 133]. For STO(001)-based interfaces, it has been proposed that different coupling between the localized magnetic moments and the $3d_{xy}$ and $3d_{xz/yz}$ electrons, due to the different orbital orientation relatively to the interface plane, can explain various magnetotransport properties of STO-structures, including a gate tunable Kondo-like minimum, AHE, and behavior of the in-plane magnetoresistance (*MR*) [90, 96]. Nevertheless, the mechanism for invoking AHE is still a matter of debate. Some studies find an induced AHE in structures with external magnetic delta doping [132, 133], in which case the presence of magnetism can be readily argued. Others find AHE also in systems without magnetic ions and suggest a mechanism arising from the properties of the STO [91, 96]. Also the Kondo-picture proposed by Refs. [90, 96] has been challenged. It was argued that enhanced spin-orbit coupling (SOC) at low temperature can produce some features of the in-plane *MR* which previously have been interpreted in favor of the picture supporting Kondo behaviour [98].

This work aims to study the gate-tunable magnetic interactions. We choose as a starting point the first reported delta-doped system, $LaAlO_3/EuTiO_3$/STO (LAO/ETO/STO). This system is reported to be ferromagnetic [132, 139] and to exhibit both tunable AHE and Kondo-like behavior. Bulk $EuTiO_3$ is an antiferromagnetic band insulator [175–181]. The oxidation state of Eu is Eu^{2+}; therefore, Ti is in the tetravalent state and does not contribute to the magnetization. However, doping with La will lead to the development of ferromagnetism [145, 192], because La is in La^{3+}state, and the doping introduces electrons into the conduction band of the $3d$ t_{2g} states of the Ti, turning ETO in ferromagnetic metal [145, 192]. In our work, to understand the role of magnetic doping on magnetic interactions, we also investigated nominally non-magnetic LAO/STO and LAO/$Eu_{1-x}La_xTiO_3$/STO (LAO/ELTO/STO).

We have prepared a set of LAO/STO samples with and without ETO and ELTO δ-doping layers and utilized a back gate geometry to study them. We observe that AHE is stronger in samples with a higher concentration of Eu moments and we find a transition between tunable AHE and Kondo-like regimes. Nevertheless, unlike the AHE, the Kondo-like regime seems to be present even in non-doped samples. We come to the conclusion that gate-tunable Kondo-like resistance behavior is not a sign of magnetic interactions, but most likely the result of the interplay between the electron trapping mechanism and the temperature dependence of STO permittivity, the carrier concentration, and various scattering mechanisms. The combination of these effects leads to more effective back gating at low temperatures and therefore to an increase in resistance.

6.2. Experimental details

The oxide structures have been grown by Pulsed Laser Deposition (PLD) on TiO_2-terminated (001)-oriented STO. In the literature, two types of targets have been used to grow ETO, the pyrochlore material $Eu_2Ti_2O_7$ [139, 147, 148, 272–274], and the perovskite material $EuTiO_3$ [146, 150, 189, 275]. In this work, we choose to work with the latter. The PLD targets for ETO and $Eu_{0.9}La_{0.1}TiO_3$ were fabricated from sintered and pressed powders [1]. The LAO target was commercially purchased. The La doping was chosen at 10% to ensure a significant difference between intentionally doped films and unintentional doping due to possible intermixing. Some significant optimization of the growth parameters was required. In order to prevent bulk conductivity of the STO due to oxygen depletion at the high growth temperatures, some oxygen in the PLD chamber is needed, but the oxygen pressure should not be too high otherwise the ETO and ELTO films turn into an amorphous or form a pyrochlore structure.

For ETO and ELTO, the laser spot size was fixed at 1.38 mm^2. For optimisation, we used a fixed thickness of 10 unit cells (u.c.) determined from the periodicity of visible specular beam intensity oscillations using Reflection High-Energy Electron Diffraction (RHEED). Fig. 6.1a shows the number of visible oscillations plotted against growth temperature for the laser fluences 1.1 and 1.54 J/cm^2. The maximum number of visible oscillations is 4, in the temperature range 750-800 °C and at a nominal pressure 1×10^{-4} mbar. Above 4 u.c. thickness, the films re-

[1] The targets were prepared by Dr. Yingkai Huang at the University of Amsterdam

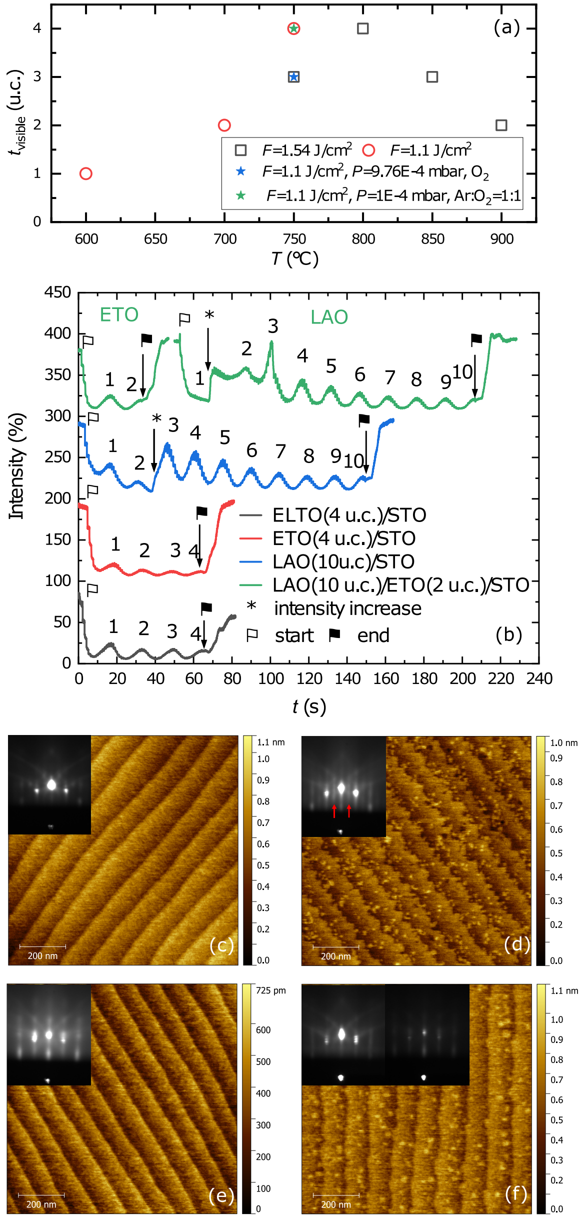

Figure 6.1: (a) Temperature dependence of the visible formation of unit cells extracted from RHEED intensity. If not indicated otherwise, the atmosphere was O_2, and the pressure was 1×10^{-4}. (b) RHEED intensity monitoring. (c)-(f) AFM image of surfaces of TiO_2-terminated STO, ETO(4 u.c.)/STO, LAO/STO, and LAO/ELTO(2 u.c.)/STO correspondingly. On the inserts corresponding RHEED patterns after deposition. Red arrows are guides for the eye. Note on the last insert left RHEED pattern after deposition of ELTO, the right one after LAO.

sult mostly in an amorphous pattern (Fig. 6.8 in the Appendix 6.6), although the samples grown at 1.54 J/cm^2 and 800 °C show some weak signatures of 2D growth (Fig. 6.8a in Appendix 6.6). Still, 4 u.c. is enough to study delta-doped LAO/STO structures. Based on the results above, we chose a fluence of 1.54 J/cm^2 for ETO and ELTO. For LAO a growth fluence of 1.3 J/cm^2 and a spot size of 1.76 mm^2 were used. The temperature was set at 800 °C and the pressure, consisting of a 1:1 mix of Ar:O_2, at 1×10^{-4} mbar. The maximum thickness of $Eu_{1\text{-}x}La_xTiO_3$ layer was fixed at 4 u.c. The following samples were grown (the numeral denoting number of u.c.'s): LAO(10)/ETO(x)/STO (with x= 2, 3, 4), LAO(10)/ELTO(x)/STO (with x=2, 4), ELTO(4)/STO, ETO(4)/STO and LAO(10)/STO.

ETO and ELTO show similar growth. The oscillations are clearly visible for ETO(4)/STO and ELTO(4)/STO samples, as shown in Fig. 6.1b (black and red lines). The RHEED pattern for ETO(4)/STO shows additional lines at the 1/2 position between the main lines for films with $t > 2$ u.c. (insert in Fig. 6.1d); such lines have been observed for stoichiometric $Eu_{1\text{-}x}La_xTiO_3$ films [149]. The STO surface steps can been clearly seen in the Atomic Force Microscopy (AFM) scan before and after growth (Fig. 6.1c,d), but the edges became more rough than on the bare STO surface. Moreover, there are island-like features in the topography of the film. During the growth of LAO, clear oscillations are seen when growing directly on STO (blue line in Fig. 6.1b). The RHEED pattern shows a transition from 2D growth to 3D growth (insert in Fig. 6.1e), most likely due to the low oxygen pressure. A clear underlying STO step pattern can be seen in the AFM scan in Fig. 6.1e. This is different when the LAO layer is grown on ETO or ELTO films. In Fig. 6.1b (green line) the first two oscillations during LAO growth become less pronounced, and their intensity decreases with the increase of the ETO or ELTO layer thickness. The thickness of the LAO layer was determined from the number of pulses for a single period of oscillations and, strictly speaking, can vary between 8 and 10 u.c. That variation is not crucial for the conductivity of LAO/$EuTiO_3$/STO, in contrast to the thickness of the ETO layer [139]. The LAO layer grown on the ETO or ELTO also shows 3D features in the RHEED pattern, but the 2D features are more pronounced. The underlying topography of ETO/ELTO films can still been seen after depositing the LAO layers. The AFM scans and RHEED patterns for the rest of the films are shown in the Appendix Fig. 6.9. The magnetotransport properties have been measured in van der Pauw geometry in a PPMS with home-built insert as described in Chapter 2.

6.3. Results

6.3.1. Metal Insulator Transition and transport properties

First we show that the behavior of our samples is similar to the ones studied in Refs. [132, 139]. Both our LAO/ETO/STO and LAO/ELTO/STO show a Metal-Insulator transition (MIT) as function of E(L)TO thickness around 2 u.c. (Fig. 6.2a), which is in agreement with the results of Ref. [139]. From now, we will refer to the two conducting samples, LAO(10)/$EuTiO_3$(2)/STO and LAO(10)/$Eu_{0.9}La_{0.1}TiO_3$(2)/STO, as LAO/ETO/STO and LAO/ELTO/STO respectively. Uncapped ETO and ELTO samples were insulating, which means that La doping [145, 192] (or La intermixing in the LAO/$Eu_{1-x}La_xTiO_3$/STO) in our films is not the driving mechanism of the MIT. Furthermore, despite the lower oxygen content, the conductance of our films cannot be attributed to the conduction due to oxygen vacancies in the STO surface alone [95]; the LAO layer is essential for creating the two-dimensional electron liquid. At room temperature, LAO/STO has a lower sheet resistance R_S than LAO/ELTO/STO, which in turn is lower than that of LAO/ETO/STO. The introduction of the thin sheet of $Eu_{1-x}La_xTiO_3$ also changes the temperature dependence of R_S: the LAO/STO sample exhibits a monotonous decrease down to 3 K, whereas the delta-doped samples show an upturn below 10 K (Fig. 6.2b). Such a change in $R_S(T)$ has been reported in Ref. [139] and was attributed to a possible Kondo effect [95, 139].

6

6.3.2. Magnetotransport properties at zero gate voltage

Before applying gate voltages, we analyze the temperature dependence of the magnetotransport properties for the three conducting samples. In LAO/STO, the value of *MR* as function of an applied magnetic field out of the plane of the sample continuously increases with decreasing temperature (Fig. 6.3a). The high values of *MR*, around 50 %, and the almost linear shape in high fields below 50 K point to spatial conductance fluctuation (see Chapter 4 or [232–238]). In the doped samples, the *MR* behavior is less monotonous; *MR* increased only up to 10-12% until the temperature reaches 10 K (Fig. 6.3c,e). Below that temperature, the *MR* decreases, tracing the upturn in the temperature dependence of R_S.

Below 100 K, the Hall coefficient R_H develops a non-linearity in high fields, indicating the onset of two-band transport [36]. Furthermore, below 10 K, there is also a low-field non-linearity in the magnetically doped samples. This indicates

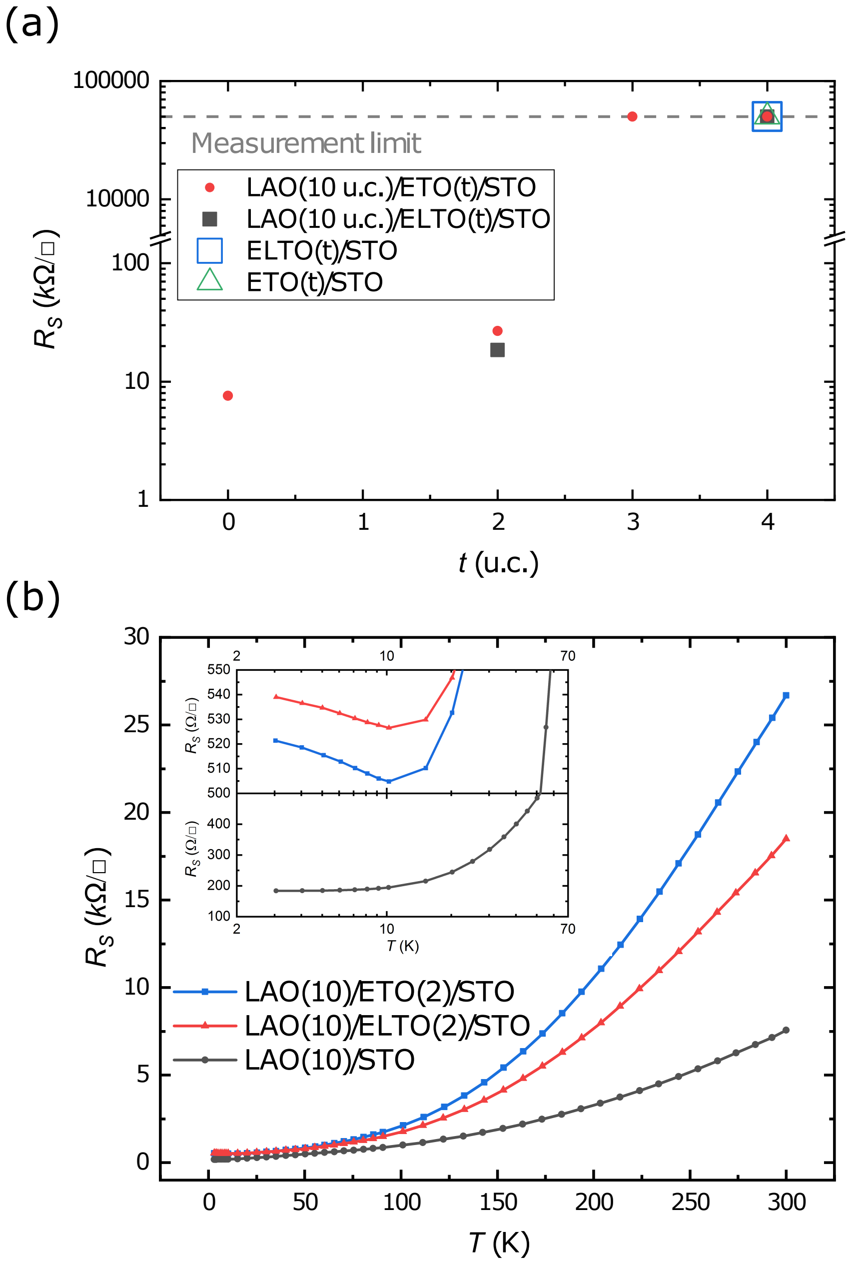

Figure 6.2: (a) The thickness dependence of the sheet resistance R_S at 300 K. (b) Temperature dependence of R_S for conducting samples. In the insert, zoom-in for the low-temperature region.

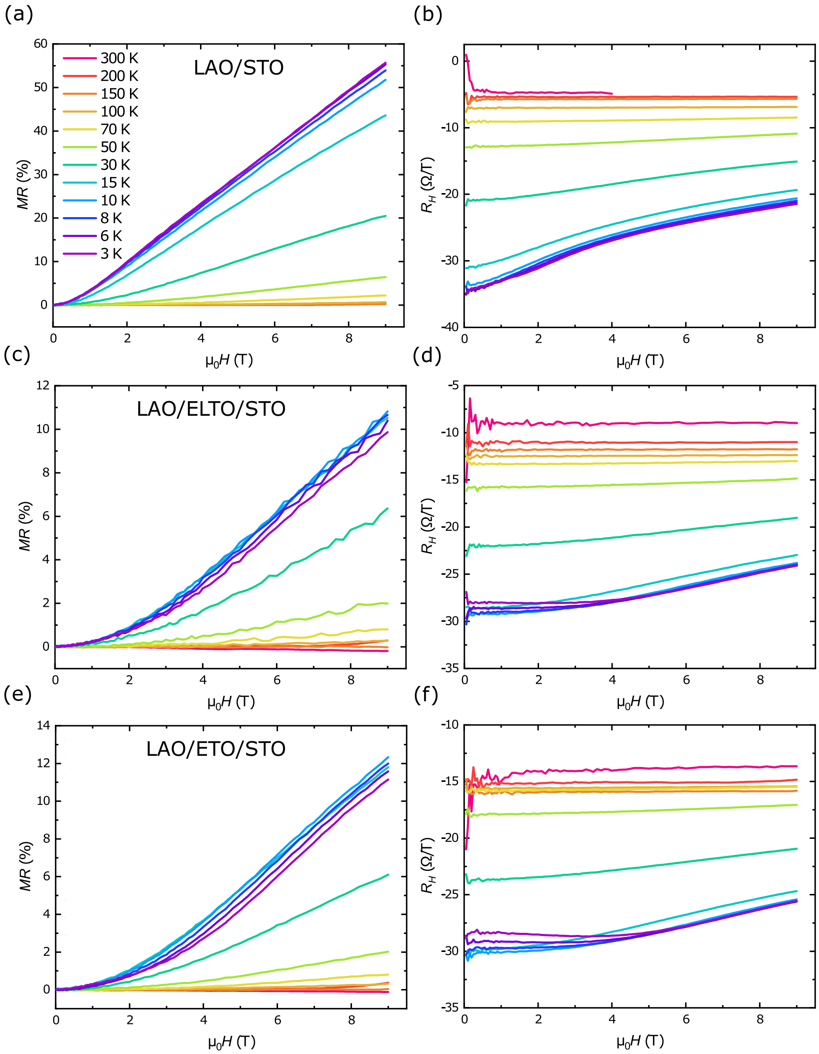

Figure 6.3: Magnetoresistance *MR* at different temperatures indicated by the colors for (a) LAO/STO, (c) LAO/ETO/STO, and (e) LAO/ELTO/STO. The Hall coefficient at different temperatures (same colors as in a,c,e) for (b) LAO/STO, (d) LAO/ETO/STO, and (f) LAO/ETO/STO.

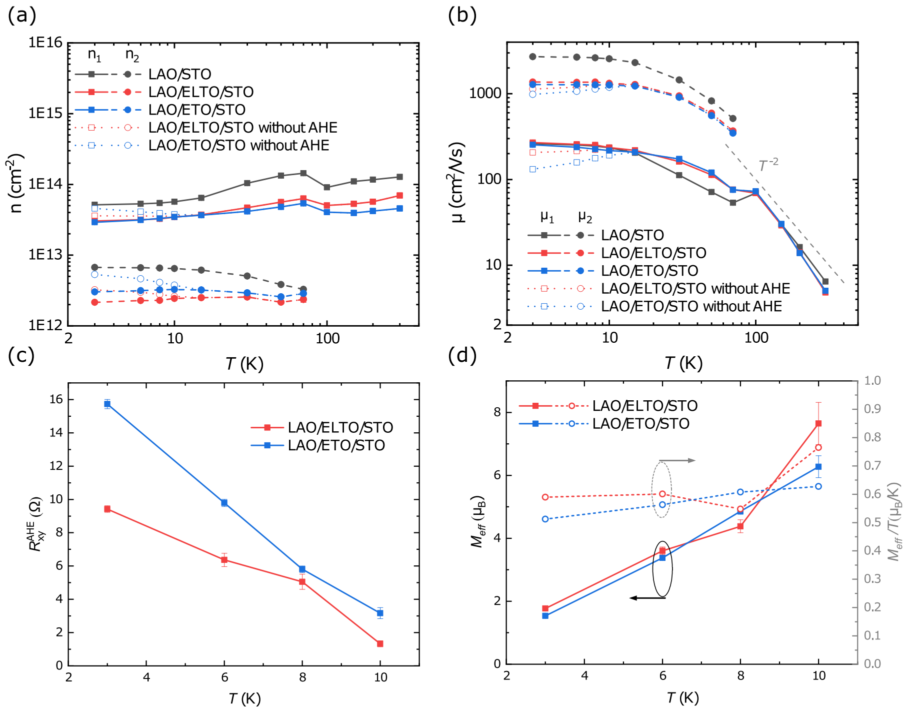

Figure 6.4: For both the LAO/STO and the LAO/E(L)TO/STO samples, the temperature dependence of (a) the carrier concentrations n_i, (b) the mobilities μ_i, (c) the Anomalous Hall coefficient, and (d) values of M_{eff} (filled symbols) and the ratio M_{eff}/T ratio (open symbols) taken from fitting as described in the text. Note that n_i and μ_i is given with and without correction for AHE when appropriate.

the presence of an Anomalous Hall Effect (AHE) [36, 91, 132] (see also Chapter 3). To analyze the data with respect to carrier densities n_i and mobilities μ_i in the presence of AHE, we followed the subtraction method described in Chapter 3 as Method 1. To increase the precision of the fit, we used the derivative of the subtraction result to determine the fitting range. The two-band analysis in a regime without AHE was performed using the fitting of the conductance tensor components [37] (also Section 3.3.5). The extracted values for n_i, μ_i, and for the Anomalous Hall coefficient R_{xy}^{AHE}, and the effective magnetic moment M_{eff} are shown in Fig. 6.4. Also shown are the values for n_i, μ_i when no AHE is taken into account. We see that in the one band region, the mobility of the samples roughly follows a T^{-2} dependence in the temperature range 150-50 K (Fig. 6.4b). The temperature dependence above 150 K is often ascribed to longitudinal optical phonon scattering, and the origin of T^{-2} mobility dependence is usually attributed to electron-electron scattering [276, 277]. As was mentioned above, the second band appears below 100 K. Some unphysical jumps are probably related to the low carrier concentration of the second band leading to overestimating (underestimating) the carrier concentration (mobility) for both type of carriers. Overall it is clear that the trend is an increase of $\mu_{1,2}$ towards low temperatures with saturation below 10 K and a continuous although small decrease of n_1. The saturation of the mobility at a low-temperature limit is most likely due to the interface, to ionized donors, and to ionized impurity scattering [276]. In the fit without the AHE, with decreasing temperature we see an increase in carrier concentration and an decrease in mobility for the magnetically doped samples below 10 K. However, when accounting for the AHE, the fits become consistent with the general trend of LAO/STO. The AHE grows when lowering the temperature, but we see that the fit parameter M_{eff} decreases almost linearly with temperature as can be seen better from the ratio M_{eff}/T. This is quite counterintuitive. If M_{eff} would simply represent the saturation magnetization of a ferromagnetically ordering interface, the trend should be opposite. Since an ordering temperature of around 10 K is expected, this points to a different interpretation of M_{eff}, which may not be surprising, since the AHE depens on more than the magnetization alone, with SOC to start with. It does not affect the determination of R_{xy}^{AHE} and the shape of the function used.

6.3.3. Gate tuning of the Anomalous Hall Effect

We have studied both the temperature and gate dependence of the AHE in doped samples. First, we consider the behavior of LAO/ETO/STO. All in all, the results are similar to those of previous AHE studies in the two-band regime in the oxide interfaces [36, 132, 135, 191]. The Lifshitz point [36] is located near 25 V, carri-

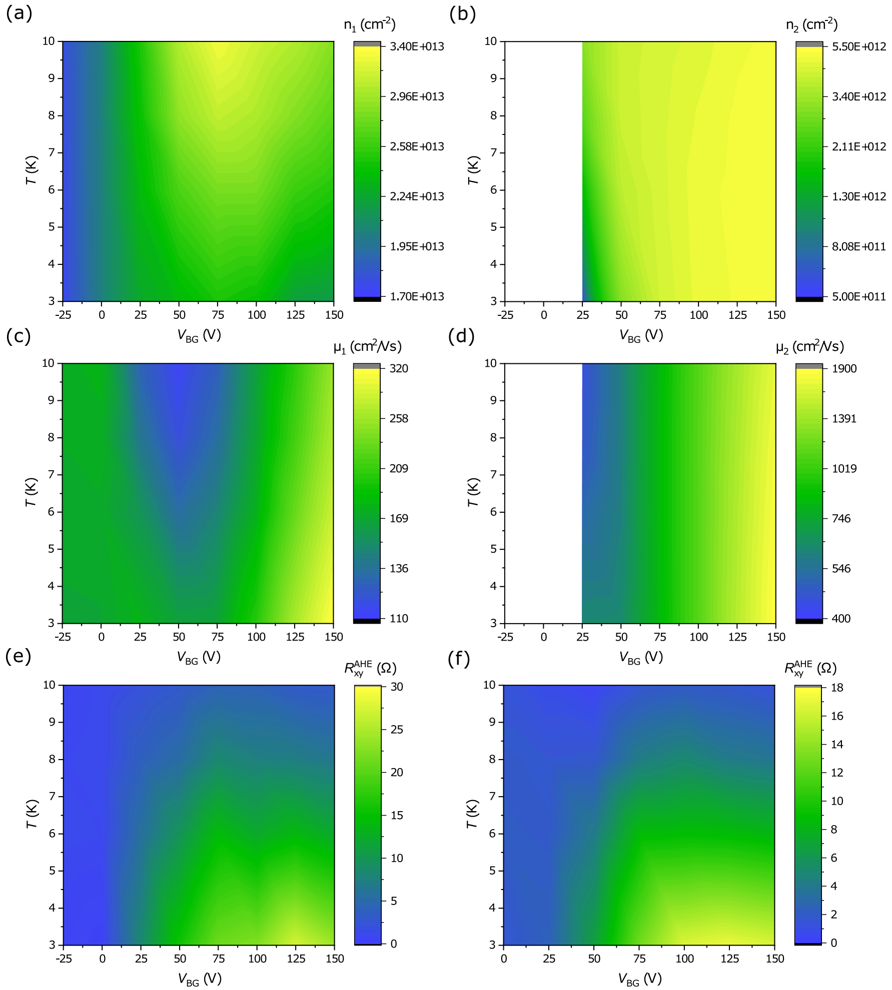

Figure 6.5: Temperature and back gate voltage dependence of (a-b) carrier concentrations, (c-d) mobilities, (e) Anomalous Hall coefficient for the LAO/ETO/STO sample. (f) Anomalous Hall coefficient for the LAO/ELTO/STO sample. The color scale for all quantities gives the range of their values.

ers of the second type appear above that voltage, see Fig. 6.5b. Unlike the carrier concentration and mobility of the low mobile carriers (Fig. 6.5a,c), the carrier concentration and mobility of the high mobile carriers (Fig. 6.5b,d) are less sensitive to a change in temperature. On the other hand, the change in voltage affects n_i and μ_i much stronger. The behavior is qualitatively the same for both samples; numbers for LAO/ELTO/STO can be found in the Appendix Fig. 6.10. The AHE disappears in the region where two-band behavior is disappearing, as would be expected in the picture where the AHE is simply controlled by the second type of carriers [96]. However, R_{xy}^{AHE} also disappears above 10 K. That can be due to vanishing of the magnetization [132], of the spin-orbit coupling (Section 3), or both. Indeed we see the signature of the weak antilocalization (WAL) indicative of spin orbit coupling in the low field *MR* in all samples. For LAO/ETO/STO this is shown in Fig. 6.6a,b and for LAO/STO and LAO/ELTO/STO in Appendix Fig. 6.11 . Note that the *MR* is strongly affected by changes in gate voltage and temperature. At the same time, the AHE coefficient is higher in the sample with higher Eu concentration. Besides that, the gate voltage and temperature dependence of the AHE coefficient for LAO/ELTO/STO (Fig. 6.5f) are similar to LAO/ETO/STO.

6

In STO-based interfaces, the AHE is often attributed to skew scattering [91, 96], one of the extrinsic mechanism for the AHE [100, 103, 104], in this case in the second band [91, 96]. If that mechanism is dominant, the AHE would be sensitive to changes in the scattering time. As we pointed out, the mobilities and carrier concentration do not change dramatically with temperature but change with the back gate voltage. However, we see that the mobility of the second band increases continuously with gate voltage, whereas the AHE first increases but then enters a saturation-like regime. To illustrate this, we plot R_{xy}^{AHE} versus μ_2 in Fig. 6.6c. Again that result is in agreement with [132]. Still, it is unexpected for simple skew-scattering pictures in the high mobile band, where R_{xy}^{AHE} would be proportional to the scattering time, and therefore roughly proportional to mobility (we can ignore the change of carrier mass because it does not change significantly with back gate voltage [278]). To shed more light on the mechanism responsible for the AHE, we performed a scaling analysis of the conductivity by calculating the values for σ_{xx} and σ_{xy}, as follows [151]:

$$\sigma_{xx} = \frac{R_S}{R_S^2 + R_{xy}^{AHE^2}}, \qquad \sigma_{xy} = \frac{R_{xy}^{AHE}}{R_S^2 + R_{xy}^{AHE^2}}, \tag{6.1}$$

and then plotting them against each other. The results are shown in Fig. 6.6d for 3 K; the calculated σ_{xx} and σ_{xy} are plotted in the Appendix, Fig. 6.13, for all temperatures. We observe that σ_{xy} scales with σ_{xx} as $\sigma_{xy} \approx \sigma_{xy}^{1.8-2}$ in the region $\sigma_{xx} > 10^{-3}\ \Omega^{-1}\mathrm{m}^{-1}$. This exponent is close to the value of 1.6 observed in the scaling of ELTO metal films [151], which is often attributed to the intrinsic contribu-

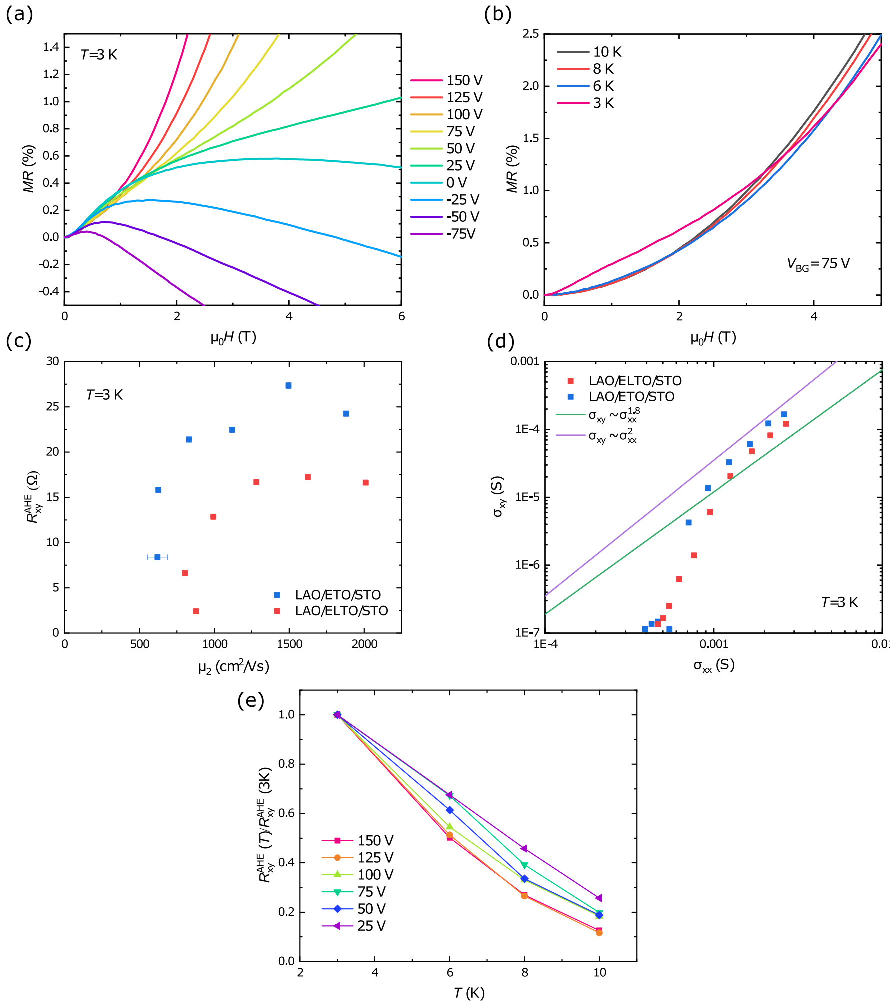

Figure 6.6: (a) Magnetoresistance *MR* with the field out of the plane at back gate voltages as indicated for LAO/ETO/STO at 3 K. (b) *MR* for LAO/ETO/STO at $V_{BG} = 75\ V$. (c) R_{xy}^{AHE} versus μ_2 for both magnetically doped samples. (d) A plot of the conductances σ_{xy} versus σ_{xx} at 3 K to investigate Scaling behavior. (e) Temperature and back gate voltage dependence of the normalized Anomalous Hall coefficient R_{xy}^{AHE} for the LAO/ELTO/STO sample.

tion to the AHE, suppressed by the disorder. Nevertheless, the meaning of scaling is somewhat limited because it corresponds to the saturation-like region, where R_{xy}^{AHE} changes less significantly than the decrease of the sheet resistance. Moreover, the interpretation of conductance scaling is often based on the ferromagnetic two-dimensional Rashba model [111, 116], where the scaling results were obtained for fixed Rashba constant. However, besides the more complex band structure in the STO-based interfaces, the Rashba constant modified with gate voltage [5, 48], as in our case can be seen from the tunable WAL effects.

A final note concerns the behavior of the fitting parameter M_{eff} in the extraction of R_{xy}^{AHE}. As seen in Appendix Fig. 6.12a,c, it shows enhancement in regions where the AHE vanishes, for instance at temperatures above 8 K and in the gate voltage range below 25 V. Most likely, the hyperbolic tangent function becomes inadequate to describe the almost flat curve. Furthermore, in most of $V_{BG} - T$ space, the ratio M_{eff}/T is only weakly temperature-dependent (Appendix Fig. 6.12b,d). Still, the point to keep in mind is that we observe the AHE in the temperature-voltage regime where the earlier studies found magnetism. A better way to establish the behavior of magnetization could be the study of the temperature dependence of the ratio $R_{xy}^{AHE}/R_{xy}^{AHE}$(3 K) because it is proportional to the temperature dependence of $M_S/M_S(3K)$ as long as carrier concentration and mobilities do not change significantly. In Fig. 6.6e, we plot $R_{xy}^{AHE}/R_{xy}^{AHE}$(3 K) at gate voltages above Lifshitz point. The ratio increases with temperature, but we do not see saturation as in Ref. [132] (note that the way in which R_{xy}^{AHE} is extracted in Ref. [132], by simple linear extrapolation, is different from ours). The temperature dependence of $R_{xy}^{AHE}/R_{xy}^{AHE}$(3 K) changes from linear at 25 V to upward curving at higher voltages. Still, as it shows a clear increase from roughly 0, it can be a signature of ferromagnetic behavior.

6.3.4. The Kondo regime in resistance

By decreasing the gate voltage below 25 V, where the AHE and the second band carrier concentration fall to zero in the magnetically doped samples, we observed the development of a minimum in the temperature dependence of the sheet resistance (Fig. 6.7a,b). That particular feature in the temperature dependence is often attributed to Kondo-like behaviour [132], which might well be connected to the magnetism of the doping layers. However, and surprisingly, we see similar behavior in nominally non-doped LAO/STO samples (Fig. 6.7c), where we do not observe AHE. It is an intriguing observation because the variation of magnetic content significantly affects the spin-polarized phase of the 2DEG, where the moment was argued to be ferromagnetically coupled with $3d_{xz/yz}$ electrons but seems not to have

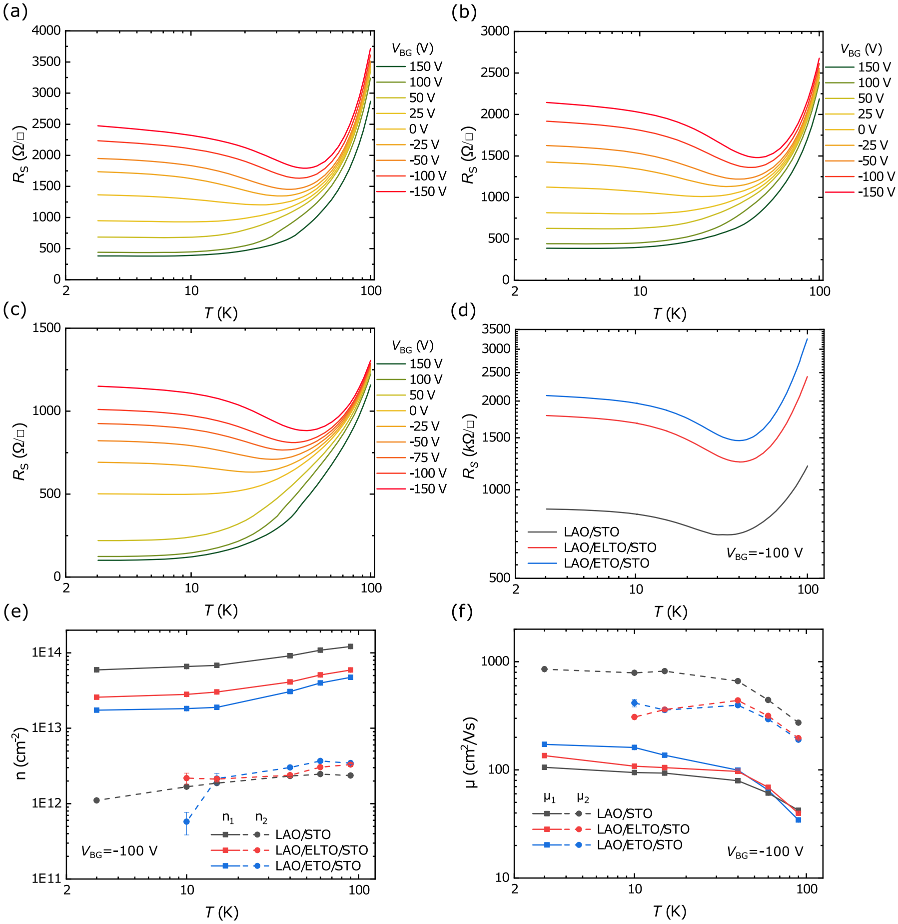

Figure 6.7: Temperature dependence of the sheet resistance R_S at different gate voltages as indicated for (a) LAO/ETO/STO, (b) LAO/ELTO/STO, and (c) LAO/STO. (d) $R_S(T)$ for all three samples measured at −100 V, (e) carrier concentration, and (f) mobility at −100 V for all three samples.

any qualitative effect on the Kondo-like regime, where moments has been argued to be antiferromagnetically coupled with $3d_{xy}$ electrons [90, 96].

To understand the nature of this behavior, we measured the temperature dependence of the sheet resistance $R_S(T)$ for all three samples at -100 V and performed magnetotransport measurements during cooldown at a few temperatures in order to find carrier concentrations and mobilities at this gate voltage. As can be seen in Fig. 6.7d, the samples show differences values of the sheet resistance but follow the same trend with a minimum around 30-40 K and saturation-like behavior below 10 K. The extracted carrier concentrations (Fig. 6.7e) from the magnetotransport data showed a constant decrease in carrier density with decreasing temperature. This is similar to the behavior of the carrier concentration of the low mobility carriers without back gate voltage, but here it is also observed for the high mobility carriers, and especially strong below 10 K. At the same time, the mobility (Fig. 6.7f) increases at first with decreasing temperature, but below 40 K saturates, in a similar way to the temperature dependence without applied back gate voltage, and can be described the same scattering picture. Important to note is that the change in the temperature dependence of the mobility happens around the temperature corresponding to the minimum in the sheet resistance.

6.4. Discussion

The results shown here are consistent with studies of LAO/ETO/STO in Ref. [132, 139, 191]. The same as in the earlier studies, we observe the MIT, the tunable AHE, the appearance of a resistance minimum and also WAL behavior. The AHE is the possible signature of ferromagnetism. Indeed, XMCD data seems to support that picture [132, 139]. Nevertheless, bulk ETO is an antiferomagnet [175–181]. It is also isostructural to STO, and, therefore, stoichiometric ETO should remain antiferromagnetic, when grown on STO [152]. At the same time, experiments revealed that antiferromagnetism only occurs for post-annealed PLD films [147, 148], and films grown by MBE [152]. Here we used PLD films without annealing, which can become ferromagnetic [147, 148, 189] because of either the formation of oxygen vacancies [147] or a longer out-of-plane lattice constant [148]. Amorphisation of ETO will also lead to the ferromagnetism [190], but in the films we studied, we do not observe, from the RHEED patterns and the intensity variations, signatures of amorphization in the films with thickness below 4 u.c. The doping with La [145, 151, 192] or oxygen deficiency [151] can also turn ETO into a ferromagnetic metal. However, the observed MIT and its weak sensitivity to the La content indicate that the occurrence of the AHE has a more complicated background than just due to ferromagnetism induced by off-stochiometry in the ETO layer. Ref. [91] observed variations of the AHE with changes in the oxygen pressure used during the growth and proposed an indirect connection between the AHE and magnetism induced by Sr vacancies rather than with external magnetic moments, including Ti^{3+} induced by oxygen vacancies. However, we used the same growth pressure for the non-doped LAO/STO sample and LAO/E(L)TO/STO, so the variation of Sr vacancies should not be too high from sample to sample. With increasing Eu content, we observe an increase of the AHE magnitude contrary to Ref. [91]. Refs. [90, 96] proposed a ferromagnetic coupling of $3d_{xz/yz}$ with localized magnetic moments such as Ti^{3+} formed due to oxygen vacancies. That indeed can explain the observation of AHE above Lifshitz point, since skew-scattering of $3d_{xz/yz}$ carriers seems to be a dominant contribution to the AHE in oxide interfaces in the two-band regime [91, 96, 132, 133]. Nevertheless, it appears to be not straightforward to explain our results on the tunable AHE. First, the AHE coefficient does not scale linearly with mobility of high mobile carriers. Second, and probably more importantly, our non-doped LAO/STO sample does not exhibit an AHE, despite the presence of $3d_{xz/yz}$ carriers. All in all, there are certainly multiple ways to induce magnetization and AHE, but in our samples magnetic doping is the main one.

In the framework of magnetic doping, we have further indication indication that the picture of magnetic interactions based purely on the symmetry of orbitals does not hold, specifically from the data in the negative gate voltage range, where the AHE vanishes. The authors of Ref. [90, 96] argued that the coupling between mobile $3d_{xy}$ electrons and localized magnetic moments is antiferromagnetic. Strong support of this picture came from the behavior of the negative in-plane *MR*. Above the Lifshitz point, the observed large drop of (negative) in-plane *MR* was attributed to the destruction of Kondo-screening and polarisations of magnetic moments with applied field [90, 96, 97]. However, that picture was challenged by Diez *et al.* [98] who found that the negative in-plane *MR* survives up to 20 K, opposite to the expectations from the temperature-dependent Kondo picture. Furthermore, single-particle Boltzmann transport theory was sufficient to reproduce the large negative *MR* by taking into the account finite-range electrostatic impurity scattering, the anisotropic Fermi surface above the Lifshitz transition and the SOC.

In this work, we also further challenge the Kondo picture. The experiments on the LAO/STO interface performed in Ref. [99] showed that the resistance minimum could be controlled by applying hydrostatic pressure. They concluded that impurity scattering, the pressure, and the temperature dependence of the STO dielectric constant plus thermally activated charge trapping are the mechanism responsible for the resistance minimum. Although we studied the back gate voltage dependence of the sheet resistance in this work, our result can be interpreted in a somewhat similar manner. At negative gate voltages, the carrier concentration decreases in the whole temperature range, but down to 40-50 K the mobility enhances due to a decrease of electron-electron scattering. Taken together, that is the reason why we observe a decrease in the resistance down to a minimum temperature. However, with a further decrease in temperature, the change in mobility is much less steep due to various scattering mechanisms coming into play, as discussed in Sec. 6.3.2. Simultaneously, the decrease of the carrier concentration is continuous and especially pronounced for the high mobility carriers. It is not surprising then that in this region the sheet resistance starts to grow again.

Two mechanisms are responsible for the decrease in the carrier concentration. One is charge trapping [54, 55], which is less effective at high temperatures than at low temperatures. Second and probably dominant here is the complex behavior of the electric permittivity of the STO single crystal substrate at low temperatures. Indeed, at high temperatures above 40 K, the permittivity hardly changes with the applied electric field, but it does change significantly at lower temperature [279–281]. It means that the effect of back gating will be significantly more efficient in the low-temperature region. Furthermore, it is well known that back gate experiments significantly affect the carrier concentration of the second type of carriers [36, 59] at low temperatures. Below 10 K, a back gate voltage depletes, or almost depletes, the second band; therefore the saturation-like behavior in this range can be explained by the much weaker change in the mobility and carrier concentration of the low mobile carriers with temperature. Note, that our results do not exclude a possibility to induce the Kondo effect at the LAO/STO interface, but only indicate that in the back gate geometry, other effects are dominant and responsible for the resistance minimum in the temperature dependence when it occurs after the application of a gate voltage.

6.5. Conclusion

In conclusion, we have studied the LAO/STO interface with and without an inserted magnetic delta-doping layer of $Eu_{1-x}La_xTiO_3$. Our experimental results are partially in agreement with previous research on these structures [132, 139, 191]. We observe that, despite the substitution of Lanthanum for Europium, the MIT happens at 2 u.c. Moreover, the AHE is indeed induced by inserting the 2 u.c. of ETO or ELTO, and can be gate tuned. Furthermore, as an important part of our message, we find that the minimum in the sheet resistance as function of temperature, found at negative back gate voltages, and which previously has been attributed to Kondo-like behavior, rather arises from the behavior of the the carrier concentrations and mobilities of both conduction bands, and is most probably due to spinless scattering mechanisms, charge trapping, and the complex temperature and electric field dependence of the STO permittivity.

6.6. Appendix

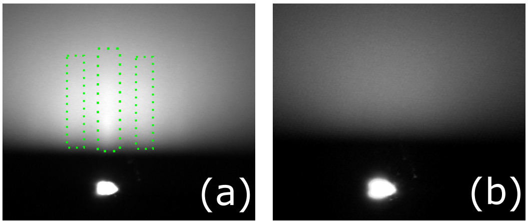

Figure 6.8: RHEED pattern after deposition of ELTO at different laser fluences F and oxygen/argoon pressures; (a) F = 1.54 J/cm^2, P_{O_2} = 1 × 10^{-4}, T = 800 °C (dotted lines are guides to the eye) and (b) F = 1.1 J/cm^2, P_{Ar+O_2} = 1 × 10^{-4}, T = 750 °C.

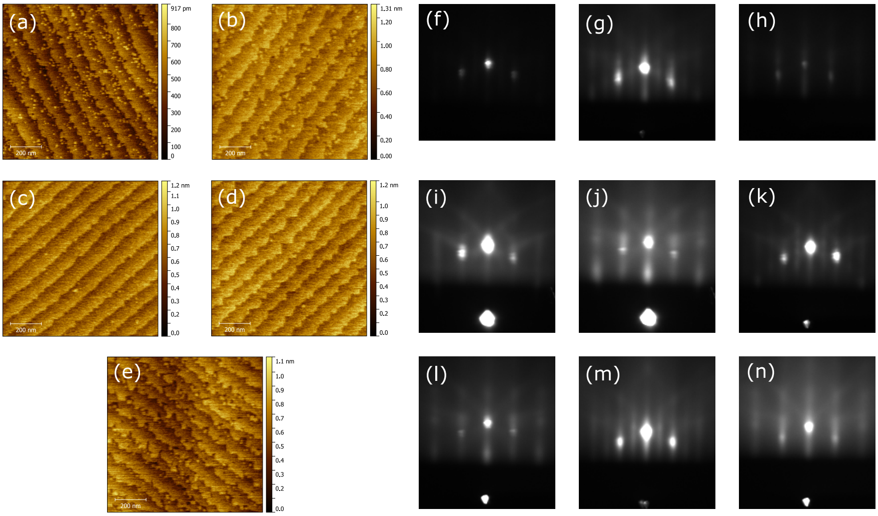

Figure 6.9: Atomic Force Microscopy (AFM) images of various sample surfaces after growth. The numerals denote the number of unit cells. (a) ELTO(4)/STO, (b) LAO/ELTO(4)/STO, (c) LAO/ETO(2)/STO, (d) LAO/ETO(3)/STO, and (e) LAO/ETO(4)/STO. RHEED patterns after deposition (f) ELTO(4)/STO, (g) and (h) LAO/ELTO(4)/STO for ELTO and LAO layers, respectively; (i) and (j) LAO/ETO(2)/STO for ETO and LAO layers respectively; (k) and (l) LAO/ETO(3)/STO for ETO and LAO layers respectively; (m) and (n) LAO/ETO(4)/STO for ETO and LAO layers, respectively.

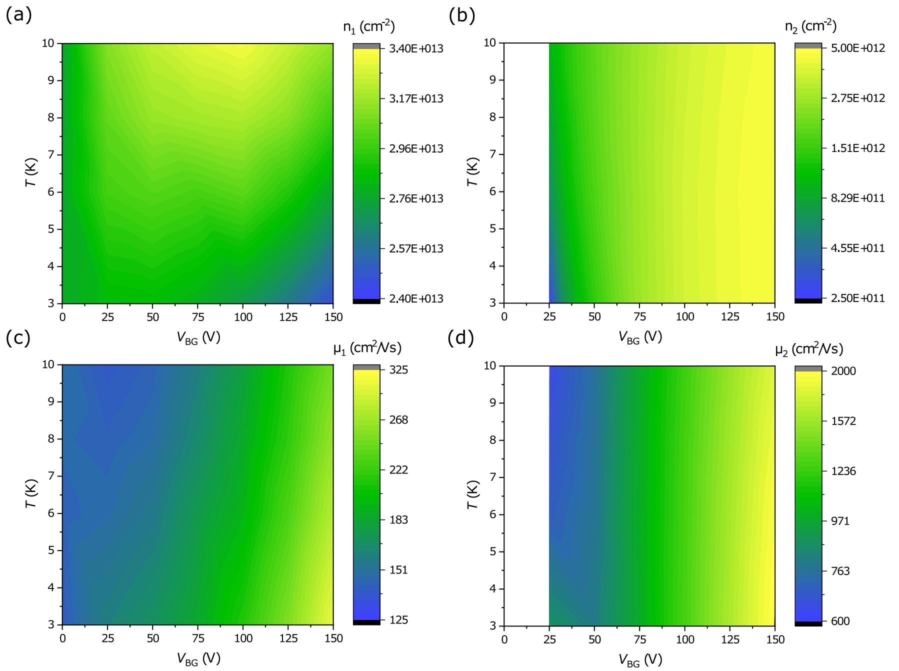

Figure 6.10: Temperature and back gate voltage dependence of (a-b) carrier concentrations and (c-d) mobilities for the LAO/ELTO/STO sample. The color scale for all quantities gives the range of their values.

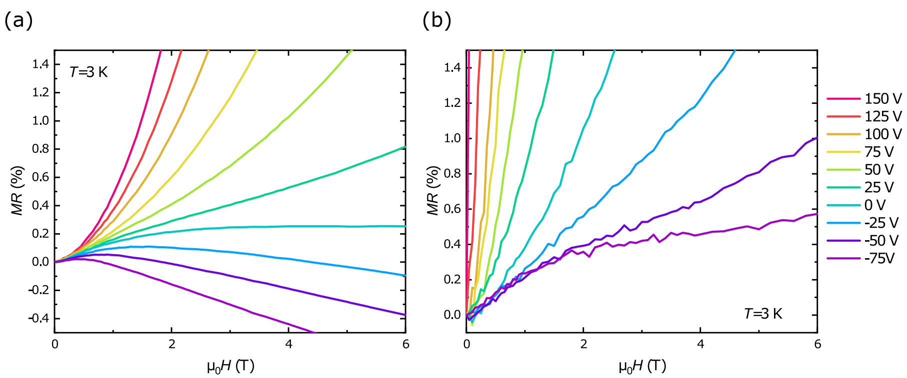

Figure 6.11: Magnetoresistance *MR* with the field out of the plane at various back gate voltages as indicated for (a) the LAO/ELTO/STO sample and (b) the LAO/STO sample at 3 K.

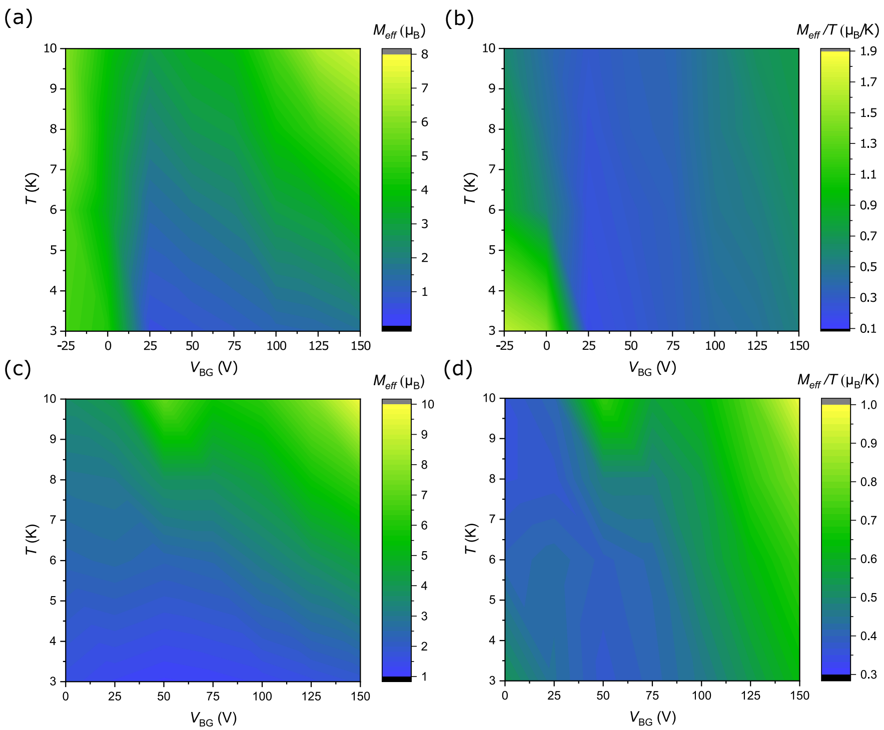

Figure 6.12: Temperature and back gate voltage dependence of the fit parameter M_{eff} for (a-b) the LAO/ETO/STO sample and (c-d) the LAO/ELTO/STO sample.

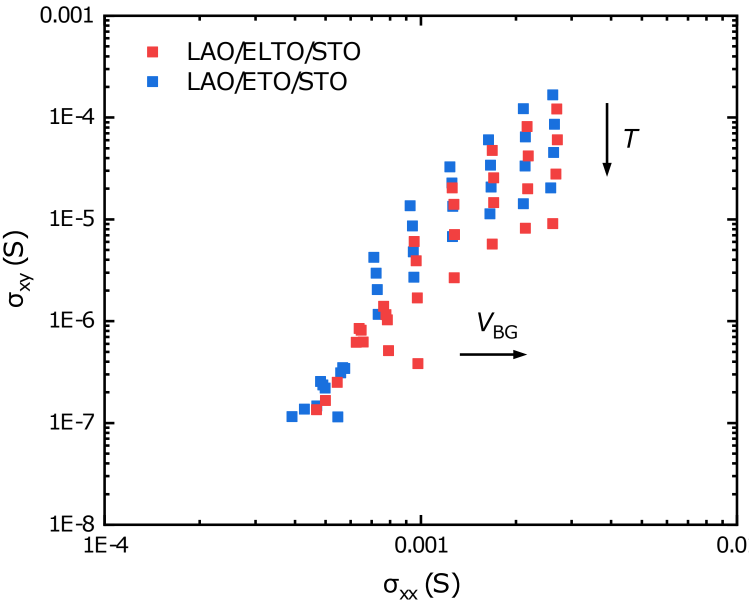

Figure 6.13: Plot of σ_{xy} versus σ_{xx} for the LAO/ETO/STO sample in order to analyze conductance scaling. Note that trend of a decrease of σ_{xy} with increasing temperature is followed poorly in the region $\sigma_{xx} < 8 \times 10^{-4}\ \Omega^{-1}\ \mathrm{m}^{-1}$.

Bibliography

[1] S. Datta and B. Das. *Electronic Analog of the Electro-Optic Modulator*. Applied Physics Letters **56**, 665–667 (1990).

[2] A. Ohtomo and H. Y. Hwang. *A High-Mobility Electron Gas at the $LaAlO_3$/$SrTiO_3$ Heterointerface*. Nature **427**, 423–426 (2004).

[3] N. Reyren, S. Thiel, A. D. Caviglia, L. F. Kourkoutis, G. Hammerl, C. Richter, C. W. Schneider, T. Kopp, A.-S. Rüetschi, D. Jaccard, M. Gabay, D. A. Muller, J.-M. Triscone, and J. Mannhart. *Superconducting Interfaces Between Insulating Oxides*. Science **317**, 1196–1199 (2007).

[4] A. D. Caviglia, S. Gariglio, N. Reyren, D. Jaccard, T. Schneider, M. Gabay, S. Thiel, G. Hammerl, J. Mannhart, and J.-M. Triscone. *Electric Field Control of the $LaAlO_3$/$SrTiO_3$ Interface Ground State*. Nature **456**, 624 (2008).

[5] A. D. Caviglia, M. Gabay, S. Gariglio, N. Reyren, C. Cancellieri, and J.-M. Triscone. *Tunable Rashba Spin-Orbit Interaction at Oxide Interfaces*. Phys. Rev. Lett. **104**, 126803 (2010).

[6] J. A. Bert, B. Kalisky, C. Bell, M. Kim, Y. Hikita, H. Y. Hwang, and K. A. Moler. *Direct Imaging of the Coexistence of Ferromagnetism and Superconductivity at the $LaAlO_3$/$SrTiO_3$ Interface*. Nature Physics **7**, 767–771 (2011).

[7] L. Li, C. Richter, J. Mannhart, and R. C. Ashoori. *Coexistence of Magnetic Order and Two-Dimensional Superconductivity at $LaAlO_3$/$SrTiO_3$ Interfaces*. Nature Physics **7**, 762 (2011).

[8] D. A. Dikin, M. Mehta, C. W. Bark, C. M. Folkman, C. B. Eom, and V. Chandrasekhar. *Coexistence of Superconductivity and Ferromagnetism in Two Dimensions*. Phys. Rev. Lett. **107**, 056802 (2011).

[9] T. Ihn. *Semiconductor Nanostructures: Quantum States and Electronic Transport*. (Oxford University Press, Oxford, 2009).

[10] Y. A. Bychkov and E. I. Rashba. *Properties of a 2D Electron Gas with Lifted Spectral Degeneracy*. Soviet Journal of Experimental and Theoretical Physics Letters **39**, 78 (1984).

[11] Y. A. Bychkov and E. I. Rashba. *Oscillatory Effects and the Magnetic Susceptibility of Carriers in Inversion Layers*. Journal of Physics C: Solid State Physics **17**, 6039–6045 (1984).

[12] G. Herranz, G. Singh, N. Bergeal, A. Jouan, J. Lesueur, J. Gázquez, M. Varela, M. Scigaj, N. Dix, F. Sánchez, and J. Fontcuberta. *Engineering Two-Dimensional Superconductivity and Rashba Spin-Orbit Coupling in $LaAlO_3/SrTiO_3$ Quantum Wells by Selective Orbital Occupancy*. Nature Communications **6**, 6028 (2015).

[13] S.-G. Lim, S. Kriventsov, T. N. Jackson, J. H. Haeni, D. G. Schlom, A. M. Balbashov, R. Uecker, P. Reiche, J. L. Freeouf, and G. Lucovsky. *Dielectric Functions and Optical Bandgaps of High-K Dielectrics for Metal-Oxide-Semiconductor Field-Effect Transistors by Far Ultraviolet Spectroscopic Ellipsometry*. Journal of Applied Physics **91**, 4500–4505 (2002).

[14] M. Cardona. *Optical Properties and Band Structure of $SrTiO_3$ and $BaTiO_3$*. Phys. Rev. **140**, A651–A655 (1965).

[15] L. F. Mattheiss. *Energy Bands for $KNiF_3$, $SrTiO_3$, $KMoO_3$, and $KTaO_3$*. Phys. Rev. B **6**, 4718–4740 (1972).

[16] H. Unoki and T. Sakudo. *Electron Spin Resonance of Fe^{3+} in $SrTiO_3$ with Special Reference to the 110°K Phase Transition*. Journal of the Physical Society of Japan **23**, 546–552 (1967).

[17] R. A. Cowley. *The Phase Transition of Strontium Titanate*. Philosophical Transactions: Mathematical, Physical and Engineering Sciences **354**, 2799–2814 (1996).

[18] N. Nakagawa, H. Y. Hwang, and D. A. Muller. *Why Some Interfaces Cannot Be Sharp*. Nature Materials **5**, 204–209 (2006).

[19] S. Gariglio, M. Gabay, and J.-M. Triscone. *Research Update: Conductivity and Beyond at the $LaAlO_3/SrTiO_3$ Interface*. APL Materials **4**, 060701 (2016).

[20] S. Thiel, G. Hammerl, A. Schmehl, C. W. Schneider, and J. Mannhart. *Tunable Quasi-Two-Dimensional Electron Gases in Oxide Heterostructures*. Science **313**, 1942–1945 (2006).

[21] L. Yu and A. Zunger. *A Polarity-Induced Defect Mechanism for Conductivity and Magnetism at Polar-Nonpolar Oxide Interfaces*. Nature Communications **5**, 5118 (2014).

[22] P. R. Willmott, S. A. Pauli, R. Herger, C. M. Schlepütz, D. Martoccia, B. D. Patterson, B. Delley, R. Clarke, D. Kumah, C. Cionca, and Y. Yacoby. *Structural Basis for the Conducting Interface between $LaAlO_3$ and $SrTiO_3$*. Phys. Rev. Lett. **99**, 155502 (2007).

[23] G. Herranz, M. Basletić, M. Bibes, C. Carrétéro, E. Tafra, E. Jacquet, K. Bouzehouane, C. Deranlot, A. Hamzić, J.-M. Broto, A. Barthélémy, and A. Fert. *High Mobility in $LaAlO_3/SrTiO_3$ Heterostructures: Origin, Dimensionality, and Perspectives*. Phys. Rev. Lett. **98**, 216803 (2007).

[24] A. Kalabukhov, R. Gunnarsson, J. Börjesson, E. Olsson, T. Claeson, and D. Winkler. *Effect of Oxygen Vacancies in the $SrTiO_3$ Substrate on the Electrical Properties of the $LaAlO_3$/$SrTiO_3$ Interface*. Phys. Rev. B **75**, 121404 (2007).

[25] Z. Q. Liu, C. J. Li, W. M. Lü, X. H. Huang, Z. Huang, S. W. Zeng, X. P. Qiu, L. S. Huang, A. Annadi, J. S. Chen, J. M. D. Coey, T. Venkatesan, and Ariando. *Origin of the Two-Dimensional Electron Gas at $LaAlO_3$/$SrTiO_3$ Interfaces: The Role of Oxygen Vacancies and Electronic Reconstruction*. Phys. Rev. X **3**, 021010 (2013).

[26] Y. Chen, N. Pryds, J. E. Kleibeuker, G. Koster, J. Sun, E. Stamate, B. Shen, G. Rijnders, and S. Linderoth. *Metallic and Insulating Interfaces of Amorphous $SrTiO_3$-Based Oxide Heterostructures*. Nano Letters **11**, 3774–3778 (2011).

[27] L. W. van Heeringen, G. A. de Wijs, A. McCollam, J. C. Maan, and A. Fasolino. *$k{\cdot}p$ Subband Structure of the $LaAlO_3$/$SrTiO_3$ Interface*. Phys. Rev. B **88**, 205140 (2013).

[28] Z. Zhong, A. Tóth, and K. Held. *Theory of Spin-Orbit Coupling at $LaAlO_3$/$SrTiO_3$ Interfaces and $SrTiO_3$ Surfaces*. Phys. Rev. B **87**, 161102 (2013).

[29] A. Janotti, D. Steiauf, and C. G. Van de Walle. *Strain Effects on the Electronic Structure of $SrTiO_3$: Toward High Electron Mobilities*. Phys. Rev. B **84**, 201304 (2011).

[30] R. Bistritzer, G. Khalsa, and A. H. MacDonald. *Electronic Structure of Doped d^0 Perovskite Semiconductors*. Phys. Rev. B **83**, 115114 (2011).

[31] A. E. M. Smink. *Manifold Field Effects at a Complex Oxide Interface*. PhD thesis (2019).

[32] L. W. van Heeringen, A. McCollam, G. A. de Wijs, and A. Fasolino. *Theoretical Models of Rashba Spin Splitting in Asymmetric $SrTiO_3$-Based Heterostructures*. Phys. Rev. B **95**, 155134 (2017).

[33] M. Salluzzo, J. C. Cezar, N. B. Brookes, V. Bisogni, G. M. De Luca, C. Richter, S. Thiel, J. Mannhart, M. Huijben, A. Brinkman, G. Rijnders, and G. Ghiringhelli. *Orbital Reconstruction and the Two-Dimensional Electron Gas at the $LaAlO_3$/$SrTiO_3$ Interface*. Phys. Rev. Lett. **102**, 166804 (2009).

[34] G. Khalsa and A. H. MacDonald. *Theory of the $SrTiO_3$ Surface State Two-Dimensional Electron Gas*. Phys. Rev. B **86**, 125121 (2012).

[35] P. D. C. King, S. McKeown Walker, A. Tamai, A. de la Torre, T. Eknapakul, P. Buaphet, S.-K. Mo, W. Meevasana, M. S. Bahramy, and F. Baumberger. *Quasiparticle Dynamics and Spin-Orbital Texture of the $SrTiO_3$ Two-Dimensional Electron Gas*. Nature Communications **5**, 3414 (2014).

[36] A. Joshua, S. Pecker, J. Ruhman, E. Altman, and S. Ilani. *A Universal Critical Density Underlying the Physics of Electrons at the $LaAlO_3$/$SrTiO_3$ Interface*. Nature Communications **3**, 1129 (2012).

[37] A. E. M. Smink, J. C. de Boer, M. P. Stehno, A. Brinkman, W. G. van der Wiel, and H. Hilgenkamp. *Gate-Tunable Band Structure of the $LaAlO_3-SrTiO_3$ Interface*. Phys. Rev. Lett. **118**, 106401 (2017).

[38] B. L. Altshuler, D. Khmel'nitzkii, A. I. Larkin, and P. A. Lee. *Magnetoresistance and Hall Effect in a Disordered Two-Dimensional Electron Gas*. Phys. Rev. B **22**, 5142–5153 (1980).

[39] Y. Araki, G. Khalsa, and A. H. MacDonald. *Weak Localization, Spin Relaxation, and Spin Diffusion: Crossover Between Weak and Strong Rashba Coupling Limits*. Phys. Rev. B **90**, 125309 (2014).

[40] C. Beenakker and H. van Houten, *Quantum Transport in Semiconductor Nanostructures*, in *Semiconductor heterostructures and nanostructures*, Vol. 44, edited by H. Ehrenreich and D. Turnbull, Solid State Physics (Academic Press, 1991), pp. 1 –228.

[41] S. Hikami, A. I. Larkin, and Y. Nagaoka. *Spin-Orbit Interaction and Magnetoresistance in the Two Dimensional Random System*. Progress of Theoretical Physics **63**, 707–710 (1980).

[42] G. Bergmann. *Weak Anti-Localization - An Experimental Proof for the Destructive Interference of Rotated Spin* 1/2. Solid State Communications **42**, 815 –817 (1982).

[43] P. Seiler, E. Lettl, D. Braak, and T. Kopp. *Weak Antilocalization within a Genuine Multiband Model*. Phys. Rev. B **100**, 115415 (2019).

[44] D. Stornaiuolo, S. Gariglio, A. Fête, M. Gabay, D. Li, D. Massarotti, and J.-M. Triscone. *Weak Localization and Spin-Orbit Interaction in Side-Gate Field Effect Devices at the $LaAlO_3$/$SrTiO_3$ Interface*. Phys. Rev. B **90**, 235426 (2014).

[45] S. Hurand, A. Jouan, C. Feuillet-Palma, G. Singh, J. Biscaras, E. Lesne, N. Reyren, A. Barthélémy, M. Bibes, J. E. Villegas, C. Ulysse, X. Lafosse, M. Pannetier-Lecoeur, S. Caprara, M. Grilli, J. Lesueur, and N. Bergeal. *Field-Effect Control of Superconductivity and Rashba Spin-Orbit Coupling in Top-Gated $LaAlO_3$/$SrTiO_3$ Devices*. Scientific Reports **5**, 12751 (2015).

[46] C. Yin, P. Seiler, L. M. K. Tang, I. Leermakers, N. Lebedev, U. Zeitler, and J. Aarts. *Tuning Rashba Spin-Orbit Coupling at $LaAlO_3$/$SrTiO_3$ Interfaces by Band Filling*. Phys. Rev. B **101**, 245114 (2020).

[47] M. Ben Shalom, M. Sachs, D. Rakhmilevitch, A. Palevski, and Y. Dagan. *Tuning Spin-Orbit Coupling and Superconductivity at the $SrTiO_3$/$LaAlO_3$ Interface: A Magnetotransport Study*. Phys. Rev. Lett. **104**, 126802 (2010).

[48] H. Liang, L. Cheng, L. Wei, Z. Luo, G. Yu, C. Zeng, and Z. Zhang. *Nonmonotonically Tunable Rashba Spin-Orbit Coupling by Multiple-Band Filling Control in $SrTiO_3$-Based Interfacial d-Electron Gases.* Phys. Rev. B **92**, 075309 (2015).

[49] E. Lesne, Y. Fu, S. Oyarzun, J. C. Rojas-Sánchez, D. C. Vaz, H. Naganuma, G. Sicoli, J.-P. Attané, M. Jamet, E. Jacquet, J.-M. George, A. Barthélémy, H. Jaffrès, A. Fert, M. Bibes, and L. Vila. *Highly Efficient and Tunable Spin-to-Charge Conversion through Rashba Coupling at Oxide Interfaces.* Nature Materials **15**, 1261 (2016).

[50] H. Nakamura, T. Koga, and T. Kimura. *Experimental Evidence of Cubic Rashba Effect in an Inversion-Symmetric Oxide.* Phys. Rev. Lett. **108**, 206601 (2012).

[51] A. E. M. Smink, M. P. Stehno, J. C. de Boer, A. Brinkman, W. G. van der Wiel, and H. Hilgenkamp. *Correlation between Superconductivity, Band Filling, and Electron Confinement at the $LaAlO_3/SrTiO_3$ Interface.* Phys. Rev. B **97**, 245113 (2018).

[52] C. Bell, S. Harashima, Y. Kozuka, M. Kim, B. G. Kim, Y. Hikita, and H. Y. Hwang. *Dominant Mobility Modulation by the Electric Field Effect at the $LaAlO_3/SrTiO_3$ Interface.* Phys. Rev. Lett. **103**, 226802 (2009).

[53] Z. Chen, H. Yuan, Y. Xie, D. Lu, H. Inoue, Y. Hikita, C. Bell, and H. Y. Hwang. *Dual-Gate Modulation of Carrier Density and Disorder in an Oxide Two-Dimensional Electron System.* Nano Letters **16**, 6130–6136 (2016).

[54] J. Biscaras, S. Hurand, C. Feuillet-Palma, A. Rastogi, R. C. Budhani, N. Reyren, E. Lesne, J. Lesueur, and N. Bergeal. *Limit of the Electrostatic Doping in Two-Dimensional Electron Gases of $LaXO_3(X = Al, Ti)/SrTiO_3$.* Scientific Reports **4**, 6788 (2014).

[55] C. Yin, A. E. M. Smink, I. Leermakers, L. M. K. Tang, N. Lebedev, U. Zeitler, W. G. van der Wiel, H. Hilgenkamp, and J. Aarts. *Electron Trapping Mechanism in $LaAlO_3/SrTiO_3$ Heterostructures.* Phys. Rev. Lett. **124**, 017702 (2020).

[56] M. Hosoda, Y. Hikita, H. Y. Hwang, and C. Bell. *Transistor Operation and Mobility Enhancement in Top-Gated $LaAlO_3/SrTiO_3$ Heterostructures.* Applied Physics Letters **103**, 103507 (2013).

[57] N. Reyren, S. Gariglio, A. D. Caviglia, D. Jaccard, T. Schneider, and J.-M. Triscone. *Anisotropy of the Superconducting Transport Properties of the $LaAlO_3/SrTiO_3$ Interface.* Applied Physics Letters **94**, 112506 (2009).

[58] G. Singh, A. Jouan, L. Benfatto, F. Couëdo, P. Kumar, A. Dogra, R. C. Budhani, S. Caprara, M. Grilli, E. Lesne, A. Barthélémy, M. Bibes, C. Feuillet-Palma, J. Lesueur, and N. Bergeal. *Competition between Electron Pairing and Phase Coherence in Superconducting Interfaces*. Nature Communications **9**, 407 (2018).

[59] J. Biscaras, N. Bergeal, S. Hurand, C. Grossetête, A. Rastogi, R. C. Budhani, D. LeBoeuf, C. Proust, and J. Lesueur. *Two-Dimensional Superconducting Phase in $LaTiO_3/SrTiO_3$ Heterostructures Induced by High-Mobility Carrier Doping*. Phys. Rev. Lett. **108**, 247004 (2012).

[60] S. Hurand, A. Jouan, C. Feuillet-Palma, G. Singh, E. Lesne, N. Reyren, A. Barthélémy, M. Bibes, J. E. Villegas, C. Ulysse, M. Pannetier-Lecoeur, M. Malnou, J. Lesueur, and N. Bergeal. *Top-Gated Field-Effect $LaAlO_3/SrTiO_3$ Devices Made by Ion-Irradiation*. Applied Physics Letters **108**, 052602 (2016).

[61] G. E. D. K. Prawiroatmodjo, F. Trier, D. V. Christensen, Y. Chen, N. Pryds, and T. S. Jespersen. *Evidence of Weak Superconductivity at the Room-Temperature Grown $LaAlO_3/SrTiO_3$ Interface*. Phys. Rev. B **93**, 184504 (2016).

[62] S. Caprara, M. Grilli, L. Benfatto, and C. Castellani. *Effective Medium Theory for Superconducting Layers: A Systematic Analysis Including Space Correlation Effects*. Phys. Rev. B **84**, 014514 (2011).

[63] N. Scopigno, D. Bucheli, S. Caprara, J. Biscaras, N. Bergeal, J. Lesueur, and M. Grilli. *Phase Separation from Electron Confinement at Oxide Interfaces*. Phys. Rev. Lett. **116**, 026804 (2016).

[64] S. Caprara, J. Biscaras, N. Bergeal, D. Bucheli, S. Hurand, C. Feuillet-Palma, A. Rastogi, R. C. Budhani, J. Lesueur, and M. Grilli. *Multiband Superconductivity and Nanoscale Inhomogeneity at Oxide Interfaces*. Phys. Rev. B **88**, 020504 (2013).

[65] Ariando, X. Wang, G. Baskaran, Z. Q. Liu, J. Huijben, J. B. Yi, A. Annadi, A. R. Barman, A. Rusydi, S. Dhar, Y. P. Feng, J. Ding, H. Hilgenkamp, and T. Venkatesan. *Electronic Phase Separation at the $LaAlO_3/SrTiO_3$ Interface*. Nature Communications **2**, 188 (2011).

[66] B. Kalisky, E. M. Spanton, H. Noad, J. R. Kirtley, K. C. Nowack, C. Bell, H. K. Sato, M. Hosoda, Y. Xie, Y. Hikita, C. Woltmann, G. Pfanzelt, R. Jany, C. Richter, H. Y. Hwang, J. Mannhart, and K. A. Moler. *Locally Enhanced Conductivity Due To the Tetragonal Domain Structure in $LaAlO_3/SrTiO_3$ Heterointerfaces*. Nature Materials **12**, 1091 (2013).

[67] H. Noad, E. M. Spanton, K. C. Nowack, H. Inoue, M. Kim, T. A. Merz, C. Bell, Y. Hikita, R. Xu, W. Liu, A. Vailionis, H. Y. Hwang, and K. A. Moler. *Variation in Superconducting Transition Temperature Due to Tetragonal Domains in Two-Dimensionally Doped $SrTiO_3$*. Phys. Rev. B **94**, 174516 (2016).

[68] M. Honig, J. A. Sulpizio, J. Drori, A. Joshua, E. Zeldov, and S. Ilani. *Local Electrostatic Imaging of Striped Domain Order in $LaAlO_3$/$SrTiO_3$*. Nature Materials **12**, 1112 (2013).

[69] H. J. H. Ma, S. Scharinger, S. W. Zeng, D. Kohlberger, M. Lange, A. Stöhr, X. R. Wang, T. Venkatesan, R. Kleiner, J. F. Scott, J. M. D. Coey, D. Koelle, and Ariando. *Local Electrical Imaging of Tetragonal Domains and Field-Induced Ferroelectric Twin Walls in Conducting $SrTiO_3$*. Phys. Rev. Lett. **116**, 257601 (2016).

[70] A. M. Goldman and N. Marković. *Superconductor-Insulator Transitions in the Two-Dimensional Limit*. Physics Today **51**, 39 (1998).

[71] V. F. Gantmakher and V. T. Dolgopolov. *Superconductor–Insulator Quantum Phase Transition*. Physics-Uspekhi **53**, 1–49 (2010).

[72] M. A. Steiner, N. P. Breznay, and A. Kapitulnik. *Approach to a Superconductor-to-Bose-Insulator Transition in Disordered Films*. Phys. Rev. B **77**, 212501 (2008).

[73] M. M. Mehta, D. A. Dikin, C. W. Bark, S. Ryu, C. M. Folkman, C. B. Eom, and V. Chandrasekhar. *Magnetic Field Tuned Superconductor-to-Insulator Transition at the $LaAlO_3$/$SrTiO_3$ Interface*. Phys. Rev. B **90**, 100506 (2014).

[74] M. M. Mehta, D. A. Dikin, C. W. Bark, S. Ryu, C. M. Folkman, C. B. Eom, and V. Chandrasekhar. *Evidence for Charge-Vortex Duality at the $LaAlO_3$/$SrTiO_3$ Interface*. Nature Communications **3**, 955 (2012).

[75] Y.-Y. Pai, A. Tylan-Tyler, P. Irvin, and J. Levy. *$LaAlO_3$/$SrTiO_3$: A Tale of Two Magnetisms*. (2016) arXiv:1610.00789.

[76] M. R. Fitzsimmons, N. W. Hengartner, S. Singh, M. Zhernenkov, F. Y. Bruno, J. Santamaria, A. Brinkman, M. Huijben, H. J. A. Molegraaf, J. de la Venta, and I. K. Schuller. *Upper Limit to Magnetism in $LaAlO_3$/$SrTiO_3$ Heterostructures*. Phys. Rev. Lett. **107**, 217201 (2011).

[77] J. M. D. Coey, M Venkatesan, and P Stamenov. *Surface Magnetism of Strontium Titanate*. Journal of Physics: Condensed Matter **28**, 485001 (2016).

[78] D. V. Christensen, Y. Frenkel, Y. Z. Chen, Y. W. Xie, Z. Y. Chen, Y. Hikita, A. Smith, L. Klein, H. Y. Hwang, N. Pryds, and B. Kalisky. *Strain-Tunable Magnetism at Oxide Domain Walls*. Nature Physics **15**, 269 (2019).

[79] A. P. Petrović, A Paré, T. R. Paudel, K Lee, S Holmes, C. H. W. Barnes, A David, T Wu, E. Y. Tsymbal, and C Panagopoulos. *Emergent Vortices at a Ferromagnetic Superconducting Oxide Interface*. New Journal of Physics **16**, 103012 (2014).

[80] A. Ron, E. Maniv, D. Graf, J.-H. Park, and Y. Dagan. *Anomalous Magnetic Ground State in an $LaAlO_3/SrTiO_3$ Interface Probed by Transport through Nanowires*. Phys. Rev. Lett. **113**, 216801 (2014).

[81] Y. Ayino, P. Xu, J. Tigre-Lazo, J. Yue, B. Jalan, and V. S. Pribiag. *Ferromagnetism and Spin-Dependent Transport at a Complex Oxide Interface*. Phys. Rev. Materials **2**, 031401 (2018).

[82] V. Guduru. *Surprising Magnetotransport in Oxide Heterostructures*. PhD thesis (2014).

[83] P. Wittlich, H. Boschker, T. Asaba, L. Li, H. M. L. Noad, C. A. Watson, K. A. Moler, D. Daraselia, D. Japaridze, A. Shengelaya, J. Wang, J. Xia, and J. Mannhart. *Exploring Possible Ferromagnetism of the $LaAlO_3/SrTiO_3$ Interface*. Phys. Rev. Materials **3**, 104418 (2019).

[84] R. Pentcheva and W. E. Pickett. *Charge Localization or Itineracy at $LaAlO_3/SrTiO_3$ Interfaces: Hole Polarons, Oxygen Vacancies, and Mobile Electrons*. Phys. Rev. B **74**, 035112 (2006).

[85] K. Janicka, J. P. Velev, and E. Y. Tsymbal. *Magnetism of $LaAlO_3/SrTiO_3$ Superlattices*. Journal of Applied Physics **103**, 07B508 (2008).

[86] N. Ganguli and P. J. Kelly. *Tuning Ferromagnetism at Interfaces between Insulating Perovskite Oxides*. Phys. Rev. Lett. **113**, 127201 (2014).

[87] G. Chen and L. Balents. *Ferromagnetism in Itinerant Two-Dimensional t_{2g} Systems*. Phys. Rev. Lett. **110**, 206401 (2013).

[88] K. Michaeli, A. C. Potter, and P. A. Lee. *Superconducting and Ferromagnetic Phases in $SrTiO_3/LaAlO_3$ Oxide Interface Structures: Possibility of Finite Momentum Pairing*. Phys. Rev. Lett. **108**, 117003 (2012).

[89] S. Banerjee, O. Erten, and M. Randeria. *Ferromagnetic Exchange, Spin-Orbit Coupling and Spiral Magnetism at the $LaAlO_3/SrTiO_3$ Interface*. Nature Physics **9**, 626–630 (2013).

[90] J. Ruhman, A. Joshua, S. Ilani, and E. Altman. *Competition between Kondo Screening and Magnetism at the $LaAlO_3/SrTiO_3$ Interface*. Phys. Rev. B **90**, 125123 (2014).

[91] F. Gunkel, C. Bell, H. Inoue, B. Kim, A. G. Swartz, T. A. Merz, Y. Hikita, S. Harashima, H. K. Sato, M. Minohara, S. Hoffmann-Eifert, R. Dittmann, and H. Y. Hwang. *Defect Control of Conventional and Anomalous Electron Transport at Complex Oxide Interfaces*. Phys. Rev. X **6**, 031035 (2016).

[92] L. Weston, X. Y. Cui, S. P. Ringer, and C. Stampfl. *Density-Functional Prediction of a Surface Magnetic Phase in $SrTiO_3$ / $LaAlO_3$ Heterostructures Induced by Al Vacancies*. Phys. Rev. Lett. **113**, 186401 (2014).

[93] N. Pavlenko, T. Kopp, and J. Mannhart. *Emerging Magnetism and Electronic Phase Separation at Titanate Interfaces*. Phys. Rev. B **88**, 201104 (2013).

[94] N. Pavlenko, T. Kopp, E. Y. Tsymbal, J. Mannhart, and G. A. Sawatzky. *Oxygen Vacancies at Titanate Interfaces: Two-Dimensional Magnetism and Orbital Reconstruction*. Phys. Rev. B **86**, 064431 (2012).

[95] A. Brinkman, M. Huijben, M. van Zalk, J. Huijben, U. Zeitler, J. C. Maan, W. G. van der Wiel, G. Rijnders, D. H. A. Blank, and H. Hilgenkamp. *Magnetic Effects at the Interface between Non-Magnetic Oxides*. Nature Materials **6**, 493 (2007).

[96] A. Joshua, J. Ruhman, S. Pecker, E. Altman, and S. Ilani. *Gate-Tunable Polarized Phase of Two-Dimensional Electrons at the $LaAlO_3$ / $SrTiO_3$ Interface*. Proceedings of the National Academy of Sciences **110**, 9633–9638 (2013).

[97] M. Ben Shalom, C. W. Tai, Y. Lereah, M. Sachs, E. Levy, D. Rakhmilevitch, A. Palevski, and Y. Dagan. *Anisotropic Magnetotransport at the $SrTiO_3$ / $LaAlO_3$ Interface*. Phys. Rev. B **80**, 140403 (2009).

[98] M. Diez, A. M. R. V. L. Monteiro, G. Mattoni, E. Cobanera, T. Hyart, E. Mulazimoglu, N. Bovenzi, C. W. J. Beenakker, and A. D. Caviglia. *Giant Negative Magnetoresistance Driven by Spin-Orbit Coupling at the $LaAlO_3$ / $SrTiO_3$ Interface*. Phys. Rev. Lett. **115**, 016803 (2015).

[99] D. Fuchs, A. Sleem, R. Schäfer, A. G. Zaitsev, M. Meffert, D. Gerthsen, R. Schneider, and H. v. Löhneysen. *Incipient Localization of Charge Carriers in the Two-Dimensional Electron System in $LaAlO_3$ / $SrTiO_3$ under Hydrostatic Pressure*. Phys. Rev. B **92**, 155313 (2015).

[100] N. Nagaosa, J. Sinova, S. Onoda, A. H. MacDonald, and N. P. Ong. *Anomalous Hall Effect*. Rev. Mod. Phys. **82**, 1539–1592 (2010).

[101] E. M. Pugh. *Hall Effect and the Magnetic Properties of Some Ferromagnetic Materials*. Phys. Rev. **36**, 1503–1511 (1930).

[102] E. M. Pugh and T. W. Lippert. *Hall e.m.f. and Intensity of Magnetization*. Phys. Rev. **42**, 709–713 (1932).

[103] J. Smit. *The Spontaneous Hall Effect in Ferromagnetics I*. Physica **21**, 877 – 887 (1955).

[104] J. Smit. *The Spontaneous Hall Effect in Ferromagnetics II*. Physica **24**, 39 –51 (1958).

[105] L. Berger. *Side-Jump Mechanism for the Hall Effect of Ferromagnets.* Phys. Rev. B **2**, 4559–4566 (1970).

[106] R. Karplus and J. M. Luttinger. *Hall Effect in Ferromagnetics.* Phys. Rev. **95**, 1154–1160 (1954).

[107] N. A. Sinitsyn, A. H. MacDonald, T. Jungwirth, V. K. Dugaev, and J. Sinova. *Anomalous Hall Effect in a Two-Dimensional Dirac Band: The Link between the Kubo-Streda Formula and the Semiclassical Boltzmann Equation Approach.* Phys. Rev. B **75**, 045315 (2007).

[108] N. A. Sinitsyn. *Semiclassical Theories of the Anomalous Hall Effect.* Journal of Physics: Condensed Matter **20**, 023201 (2007).

[109] A. Crépieux and P. Bruno. *Theory of the Anomalous Hall Effect from the Kubo Formula and the Dirac Equation.* Phys. Rev. B **64**, 014416 (2001).

[110] S. Onoda, N. Sugimoto, and N. Nagaosa. *Theory of Non-Equilibirum States Driven by Constant Electromagnetic Fields: Non-Commutative Quantum Mechanics in the Keldysh Formalism.* Progress of Theoretical Physics **116**, 61–86 (2006).

[111] S. Onoda, N. Sugimoto, and N. Nagaosa. *Quantum Transport Theory of Anomalous Electric, Thermoelectric, and Thermal Hall Effects in Ferromagnets.* Phys. Rev. B **77**, 165103 (2008).

[112] M. V. Berry. *Quantal Phase Factors Accompanying Adiabatic Changes.* Proceedings of the Royal Society of London. A. Mathematical and Physical Sciences **392**, 45–57 (1984).

[113] M.-C. Chang and Q. Niu. *Berry Phase, Hyperorbits, and the Hofstadter Spectrum: Semiclassical Dynamics in Magnetic Bloch Bands.* Phys. Rev. B **53**, 7010–7023 (1996).

[114] G. Sundaram and Q. Niu. *Wave-Packet Dynamics in Slowly Perturbed Crystals: Gradient Corrections and Berry-Phase Effects.* Phys. Rev. B **59**, 14915–14925 (1999).

[115] N. A. Sinitsyn, Q. Niu, and A. H. MacDonald. *Coordinate Shift in the Semiclassical Boltzmann Equation and the Anomalous Hall Effect.* Phys. Rev. B **73**, 075318 (2006).

[116] A. A. Kovalev, Y. Tserkovnyak, K. Výborný, and J. Sinova. *Transport Theory for Disordered Multiple-Band Systems: Anomalous Hall Effect and Anisotropic Magnetoresistance.* Phys. Rev. B **79**, 195129 (2009).

[117] D. Culcer, A. MacDonald, and Q. Niu. *Anomalous Hall Effect in Paramagnetic Two-Dimensional Systems.* Phys. Rev. B **68**, 045327 (2003).

[118] I. A. Ado, I. A. Dmitriev, P. M. Ostrovsky, and M. Titov. *Anomalous Hall Effect in a 2D Rashba Ferromagnet*. Phys. Rev. Lett. **117**, 046601 (2016).

[119] A. A. Kovalev, K. Výborný, and J. Sinova. *Hybrid Skew Scattering Regime of the Anomalous Hall Effect in Rashba Systems: Unifying Keldysh, Boltzmann, and Kubo Formalisms*. Phys. Rev. B **78**, 041305 (2008).

[120] T. Kato, Y. Ishikawa, H. Itoh, and J. ichiro Inoue. *Anomalous Hall Effect in Spin-Polarized Two-Dimensional Electron Gases with Rashba Spin–Orbit Interaction*. New Journal of Physics **9**, 350–350 (2007).

[121] M. Borunda, T. S. Nunner, T. Lück, N. A. Sinitsyn, C. Timm, J. Wunderlich, T. Jungwirth, A. H. MacDonald, and J. Sinova. *Absence of Skew Scattering in Two-Dimensional Systems: Testing the Origins of the Anomalous Hall Effect*. Phys. Rev. Lett. **99**, 066604 (2007).

[122] T. S. Nunner, N. A. Sinitsyn, M. F. Borunda, V. K. Dugaev, A. A. Kovalev, A. Abanov, C. Timm, T. Jungwirth, J.-i. Inoue, A. H. MacDonald, and J. Sinova. *Anomalous Hall Effect in a Two-Dimensional Electron Gas*. Phys. Rev. B **76**, 235312 (2007).

[123] S. Onoda, N. Sugimoto, and N. Nagaosa. *Intrinsic Versus Extrinsic Anomalous Hall Effect in Ferromagnets*. Phys. Rev. Lett. **97**, 126602 (2006).

[124] A. K. Majumdar and L. Berger. *Hall Effect and Magnetoresistance in Pure Iron, Lead, Fe-Co, and Fe-Cr Dilute Alloys*. Phys. Rev. B **7**, 4203–4220 (1973).

[125] Y. Shiomi, Y. Onose, and Y. Tokura. *Extrinsic Anomalous Hall Effect in Charge and Heat Transport in Pure Iron, $Fe_{0.997}Si_{0.003}$, and $Fe_{0.97}Co_{0.03}$*. Phys. Rev. B **79**, 100404 (2009).

[126] K. Ueno, T. Fukumura, H. Toyosaki, M. Nakano, and M. Kawasaki. *Anomalous Hall Effect in Anatase $Ti_{1-x}Co_xO_{2-\delta}$ at Low Temperature Regime*. Applied Physics Letters **90**, 072103 (2007).

[127] S. Sangiao, L. Morellon, G. Simon, J. M. De Teresa, J. A. Pardo, J. Arbiol, and M. R. Ibarra. *Anomalous Hall Effect in Fe (001) Epitaxial Thin Films over a Wide Range in Conductivity*. Phys. Rev. B **79**, 014431 (2009).

[128] A. Fernández-Pacheco, J. M. De Teresa, J. Orna, L. Morellon, P. A. Algarabel, J. A. Pardo, and M. R. Ibarra. *Universal Scaling of the Anomalous Hall Effect in Fe_3O_4 Epitaxial Thin Films*. Phys. Rev. B **77**, 100403 (2008).

[129] S. H. Chun, Y. S. Kim, H. K. Choi, I. T. Jeong, W. O. Lee, K. S. Suh, Y. S. Oh, K. H. Kim, Z. G. Khim, J. C. Woo, and Y. D. Park. *Interplay between Carrier and Impurity Concentrations in Annealed $Ga_{1-x}Mn_xAs$: Intrinsic Anomalous Hall Effect*. Phys. Rev. Lett. **98**, 026601 (2007).

[130] T. Miyasato, N. Abe, T. Fujii, A. Asamitsu, S. Onoda, Y. Onose, N. Nagaosa, and Y. Tokura. *Crossover Behavior of the Anomalous Hall Effect and Anomalous Nernst Effect in Itinerant Ferromagnets.* Phys. Rev. Lett. **99**, 086602 (2007).

[131] I. A. Ado, I. A. Dmitriev, P. M. Ostrovsky, and M. Titov. *Anomalous Hall Effect with Massive Dirac Fermions.* EPL (Europhysics Letters) **111**, 37004 (2015).

[132] D. Stornaiuolo, C. Cantoni, G. M. De Luca, R. Di Capua, E. Di. Gennaro, G. Ghiringhelli, B. Jouault, D. Marrè, D. Massarotti, F. Miletto Granozio, I. Pallecchi, C. Piamonteze, S. Rusponi, F. Tafuri, and M. Salluzzo. *Tunable Spin Polarization and Superconductivity in Engineered Oxide Interfaces.* Nature Materials **15**, 278 (2015).

[133] H. R. Zhang, Y. Zhang, H. Zhang, J. Zhang, X. Shen, X. X. Guan, Y. Z. Chen, R. C. Yu, N. Pryds, Y. S. Chen, B. G. Shen, and J. R. Sun. *Magnetic Two-Dimensional Electron Gas at the Manganite-Buffered $LaAlO_3/SrTiO_3$ Interface.* Phys. Rev. B **96**, 195167 (2017).

[134] Y. Gan, D. V. Christensen, Y. Zhang, H. Zhang, D. Krishnan, Z. Zhong, W. Niu, D. J. Carrad, K. Norrman, M. von Soosten, T. S. Jespersen, B. Shen, N. Gauquelin, J. Verbeeck, J. Sun, N. Pryds, and Y. Chen. *Diluted Oxide Interfaces with Tunable Ground States.* Advanced Materials **31**, 1805970 (2019).

[135] Y. Gan, Y. Zhang, D. V. Christensen, N. Pryds, and Y. Chen. *Gate-Tunable Rashba Spin-Orbit Coupling and Spin Polarization at Diluted Oxide Interfaces.* Phys. Rev. B **100**, 125134 (2019).

[136] Y. Zhang, Y. Gan, H. Zhang, H. Zhang, P. Norby, B. Shen, J. Sun, and Y. Chen. *Metallic Conduction and Ferromagnetism in $MAl_2O_4/SrTiO_3$ Spinel/Perovskite Heterostructures (M = Fe, Co, Ni).* Applied Physics Letters **113**, 261603 (2018).

[137] Y. Cao, X. Liu, P. Shafer, S. Middey, D. Meyers, M. Kareev, Z. Zhong, J.-W. Kim, P. J. Ryan, E. Arenholz, and J. Chakhalian. *Anomalous Orbital Structure in a Spinel-Perovskite Interface.* npj Quantum Materials **1**, 16009 (2016).

[138] H. Zhang, X. Yan, H. Zhang, F. Wang, Y. Gu, X. Ning, T. Khan, R. Li, Y. Chen, W. Liu, S. Wang, B. Shen, and J. Sun. *Magnetic Two-Dimensional Electron Gases with High Curie Temperatures at $LaAlO_3/SrTiO_3$:Fe Interfaces.* Phys. Rev. B **97**, 155150 (2018).

[139] G. M. De Luca, R. Di Capua, E. Di Gennaro, F. M. Granozio, D. Stornaiuolo, M. Salluzzo, A. Gadaleta, I. Pallecchi, D. Marrè, C. Piamonteze, M. Radovic, Z. Ristic, and S. Rusponi. *Transport Properties of a Quasi-Two-Dimensional Electron System Formed in $LaAlO_3/EuTiO_3/SrTiO_3$ Heterostructures.* Phys. Rev. B **89**, 224413 (2014).

[140] J. Biscaras, N. Bergeal, A. Kushwaha, T. Wolf, A. Rastogi, R. C. Budhani, and J. Lesueur. *Two-dimensional Superconductivity at a Mott Insulator/Band Insulator Interface $LaTiO_3$ / $SrTiO_3$*. Nature Communications **1**, 89 (2010).

[141] C. He, T. D. Sanders, M. T. Gray, F. J. Wong, V. V. Mehta, and Y. Suzuki. *Metal-Insulator Transitions in Epitaxial $LaVO_3$ and $LaTiO_3$ Films.* Phys. Rev. B **86**, 081401 (2012).

[142] P. Scheiderer, M. Schmitt, J. Gabel, M. Zapf, M. Stübinger, P. Schütz, L. Dudy, C. Schlueter, T.-L. Lee, M. Sing, and R. Claessen. *Tailoring Materials for Mottronics: Excess Oxygen Doping of a Prototypical Mott Insulator.* Advanced Materials **30**, 1706708.

[143] R. Aeschlimann, D. Preziosi, P. Scheiderer, M. Sing, S. Valencia, J. Santamaria, C. Luo, H. Ryll, F. Radu, R. Claessen, C. Piamonteze, and M. Bibes. *A Living-Dead Magnetic Layer at the Surface of Ferrimagnetic $DyTiO_3$ Thin Films.* Advanced Materials **30**, 1707489.

[144] M. N. Grisolia, F. Y. Bruno, D. Sando, H. J. Zhao, E. Jacquet, X. M. Chen, L. Bellaiche, A. Barthélémy, and M. Bibes. *Structural, Magnetic, and Electronic Properties of $GdTiO_3$ Mott Insulator Thin Films Grown by Pulsed Laser Deposition.* Applied Physics Letters **105**, 172402 (2014).

[145] K. S. Takahashi, M. Onoda, M. Kawasaki, N. Nagaosa, and Y. Tokura. *Control of the Anomalous Hall Effect by Doping in $Eu_{1-x}La_xTiO_3$ Thin Films.* Phys. Rev. Lett. **103**, 057204 (2009).

[146] R. Zhao, W. W. Li, L. Chen, Q. Q. Meng, J. Yang, H. Wang, Y. Q. Wang, R. J. Tang, and H. Yang. *Conduction Mechanisms of Epitaxial $EuTiO_3$ Thin Films.* Applied Physics Letters **101**, 102901 (2012).

[147] K. Shimamoto, K. Hatabayashi, Y. Hirose, S. Nakao, T. Fukumura, and T. Hasegawa. *Full Compensation of Oxygen Vacancies in $EuTiO_3$ (001) Epitaxial Thin Film Stabilized by a $SrTiO_3$ Surface Protection Layer.* Applied Physics Letters **102**, 042902 (2013).

[148] K. Fujita, N. Wakasugi, S. Murai, Y. Zong, and K. Tanaka. *High-Quality Antiferromagnetic $EuTiO_3$ Epitaxial Thin Films on $SrTiO_3$ Prepared by Pulsed Laser Deposition and Postannealing.* Applied Physics Letters **94**, 062512 (2009).

[149] A. Shkabko, C. Xu, P. Meuffels, F. Gunkel, R. Dittmann, A. Weidenkaff, and R. Waser. *Tuning Cationic Composition of La:$EuTiO_{3-\delta}$ Films.* APL Materials **1**, 052111 (2013).

[150] H.-H. Wang, A. Fleet, J. D. Brock, D. Dale, and Y. Suzuki. *Nearly Strain-Free Heteroepitaxial System for Fundamental Studies of Pulsed Laser Deposition: $EuTiO_3$ on $SrTiO_3$*. Journal of Applied Physics **96**, 5324–5328 (2004).

[151] K. S. Takahashi, H. Ishizuka, T. Murata, Q. Y. Wang, Y. Tokura, N. Nagaosa, and M. Kawasaki. *Anomalous Hall Effect Derived from Multiple Weyl Nodes in High-Mobility $EuTiO_3$ Films*. Science Advances **4** (2018) 10.1126/sciadv.aar7880.

[152] J. H. Lee, X. Ke, N. J. Podraza, L. F. Kourkoutis, T. Heeg, M. Roeckerath, J. W. Freeland, C. J. Fennie, J. Schubert, D. A. Muller, P. Schiffer, and D. G. Schlom. *Optical Band Gap and Magnetic Properties of Unstrained $EuTiO_3$ Films*. Applied Physics Letters **94**, 212509 (2009).

[153] J. H. Lee, L. Fang, E. Vlahos, X. Ke, Y. W. Jung, L. F. Kourkoutis, J.-W. Kim, P. J. Ryan, T. Heeg, M. Roeckerath, V. Goian, M. Bernhagen, R. Uecker, P. C. Hammel, K. M. Rabe, S. Kamba, J. Schubert, J. W. Freeland, D. A. Muller, C. J. Fennie, P. Schiffer, V. Gopalan, E. Johnston-Halperin, and D. G. Schlom. *A Strong Ferroelectric Ferromagnet Created by Means of Spin-Lattice Coupling*. Nature **466**, 954–958 (2010).

[154] P. Moetakef, D. G. Ouellette, J. Y. Zhang, T. A. Cain, S. J. Allen, and S. Stemmer. *Growth and Properties of $GdTiO_3$ Films Prepared by Hybrid Molecular Beam Epitaxy*. Journal of Crystal Growth **355**, 166 –170 (2012).

[155] A. Ohtomo, D. A. Muller, J. L. Grazul, and H. Y. Hwang. *Epitaxial Growth and Electronic Structure of $LaTiO_x$ Films*. Applied Physics Letters **80**, 3922–3924 (2002).

[156] R. F. Need, B. J. Isaac, B. J. Kirby, J. A. Borchers, S. Stemmer, and S. D. Wilson. *Octahedral Tilt Independent Magnetism in Confined $GdTiO_3$ Films*. Applied Physics Letters **112**, 132407 (2018).

[157] H. D. Zhou and J. B. Goodenough. *Localized or Itinerant TiO_3 Electrons in $RTiO_3$ Perovskites*. Journal of Physics: Condensed Matter **17**, 7395 (2005).

[158] A. C. Komarek, H. Roth, M. Cwik, W.-D. Stein, J. Baier, M. Kriener, F. Bourée, T. Lorenz, and M. Braden. *Magnetoelastic Coupling in $RTiO_3$ (R =La, Nd, Sm, Gd, Y) Investigated with Diffraction Techniques and Thermal Expansion Measurements*. Phys. Rev. B **75**, 224402 (2007).

[159] M. Cwik, T. Lorenz, J. Baier, R. Müller, G. André, F. Bourée, F. Lichtenberg, A. Freimuth, R. Schmitz, E. Müller-Hartmann, and M. Braden. *Crystal and Magnetic Structure of $LaTiO_3$: Evidence for Nondegenerate t_{2g} Orbitals*. Phys. Rev. B **68**, 060401 (2003).

[160] J. Goral and J. Greedan. *The Magnetic Structures of $LaTiO_3$ and $CeTiO_3$*. Journal of Magnetism and Magnetic Materials **37**, 315 –321 (1983).

[161] G. I. Meijer, W. Henggeler, J. Brown, O.-S. Becker, J. G. Bednorz, C. Rossel, and P. Wachter. *Reduction of Ordered Moment in Strongly Correlated $LaTiO_{3+\delta}$ upon Band Filling*. Phys. Rev. B **59**, 11832–11836 (1999).

[162] F. J. Wong, S.-H. Baek, R. V. Chopdekar, V. V. Mehta, H.-W. Jang, C.-B. Eom, and Y. Suzuki. *Metallicity in $LaTiO_3$ Thin Films Induced by Lattice Deformation*. Phys. Rev. B **81**, 161101 (2010).

[163] R. Ohtsuka, M. Matvejeff, K. Nishio, R. Takahashi, and M. Lippmaa. *Transport Properties of $LaTiO_3/SrTiO_3$ Heterostructures*. Applied Physics Letters **96**, 192111 (2010).

[164] J. H. You and J. H. Lee. *Critical Thickness for the Two-Dimensional Electron Gas in $LaTiO_3/SrTiO_3$ Superlattices*. Phys. Rev. B **88**, 155111 (2013).

[165] B. Vilquin, T. Kanki, T. Yanagida, H. Tanaka, and T. Kawai. *Effect of Sr Doping on $LaTiO_3$ Thin Films*. Applied Surface Science **244**, 12th International Conference on Solid Films and Surfaces, 494 –497 (2005).

[166] Y. Tokura, Y. Taguchi, Y. Okada, Y. Fujishima, T. Arima, K. Kumagai, and Y. Iye. *Filling Dependence of Electronic Properties on the Verge of Metal–Mott-Insulator Transition in $Sr_{1-x}La_xTiO_3$*. Phys. Rev. Lett. **70**, 2126–2129 (1993).

[167] C. C. Hays, J.-S. Zhou, J. T. Markert, and J. B. Goodenough. *Electronic Transition in $La_{1-x}Sr_xTiO_3$*. Phys. Rev. B **60**, 10367–10373 (1999).

[168] S. Gariglio, J. W. Seo, J. Fompeyrine, J.-P. Locquet, and J.-M. Triscone. *Transport Properties in Doped Mott Insulator Epitaxial $La_{1-y}TiO_{3+\delta}$ Thin Films*. Phys. Rev. B **63**, 161103 (2001).

[169] J. Biscaras, N. Bergeal, S. Hurand, C. Feuillet-Palma, A. Rastogi, R. C. Budhani, M. Grilli, S. Caprara, and J. Lesueur. *Multiple Quantum Criticality in a Two-Dimensional Superconductor*. Nature Materials **12**, 542 (2013).

[170] M. J. Veit, R. Arras, B. J. Ramshaw, R. Pentcheva, and Y. Suzuki. *Nonzero Berry Phase in Quantum Oscillations from Giant Rashba-Type Spin Splitting in $LaTiO_3/SrTiO_3$ Heterostructures*. Nature Communications **9**, 1458 (2018).

[171] C. W. Turner and J. Greedan. *Ferrimagnetism in the Rare Earth Titanium (III) Oxides, $RTiO_3$; R = Gd, Tb, Dy, Ho, Er, Tm*. Journal of Solid State Chemistry **34**, 207 –213 (1980).

[172] P. Moetakef, J. Y. Zhang, A. Kozhanov, B. Jalan, R. Seshadri, S. J. Allen, and S. Stemmer. *Transport in Ferromagnetic $GdTiO_3/SrTiO_3$ Heterostructures*. Applied Physics Letters **98**, 112110 (2011).

[173] C. A. Jackson and S. Stemmer. *Interface-Induced Magnetism in Perovskite Quantum Wells*. Phys. Rev. B **88**, 180403 (2013).

[174] P. Moetakef, J. R. Williams, D. G. Ouellette, A. P. Kajdos, D. Goldhaber-Gordon, S. J. Allen, and S. Stemmer. *Carrier-Controlled Ferromagnetism in $SrTiO_3$*. Phys. Rev. X **2**, 021014 (2012).

[175] C.-L. Chien, S. DeBenedetti, and F. D. S. Barros. *Magnetic Properties of $EuTiO_3$, Eu_2TiO_4, and $Eu_3Ti_2O_7$*. Phys. Rev. B **10**, 3913–3922 (1974).

[176] T. R. McGuire, M. W. Shafer, R. J. Joenk, H. A. Alperin, and S. J. Pickart. *Magnetic Structure of $EuTiO_3$*. Journal of Applied Physics **37**, 981–982 (1966).

[177] J. Schiemer, L. J. Spalek, S. S. Saxena, C. Panagopoulos, T. Katsufuji, A. Bussmann-Holder, J. Köhler, and M. A. Carpenter. *Magnetic Field and in situ Stress Dependence of Elastic Behavior in $EuTiO_3$ from Resonant Ultrasound Spectroscopy*. Phys. Rev. B **93**, 054108 (2016).

[178] A. Bussmann-Holder, J. Köhler, R. K. Kremer, and J. M. Law. *Relation Between Structural Instabilities in $EuTiO_3$ and $SrTiO_3$*. Phys. Rev. B **83**, 212102 (2011).

[179] D. Bessas, K. Z. Rushchanskii, M. Kachlik, S. Disch, O. Gourdon, J. Bednarcik, K. Maca, I. Sergueev, S. Kamba, M. Ležaić, and R. P. Hermann. *Lattice Instabilities in Bulk $EuTiO_3$*. Phys. Rev. B **88**, 144308 (2013).

[180] D. S. Ellis, H. Uchiyama, S. Tsutsui, K. Sugimoto, K. Kato, D. Ishikawa, and A. Q. R. Baron. *Phonon Softening and Dispersion in $EuTiO_3$*. Phys. Rev. B **86**, 220301 (2012).

[181] T. Katsufuji and H. Takagi. *Coupling between Magnetism and Dielectric Properties in Quantum Paraelectric $EuTiO_3$*. Phys. Rev. B **64**, 054415 (2001).

[182] P. G. Reuvekamp, R. K. Kremer, J. Köhler, and A. Bussmann-Holder. *Evidence for the First-Order Nature of the Structural Instability in $EuTiO_3$ from Thermal Expansion Measurements*. Phys. Rev. B **90**, 104105 (2014).

[183] L. J. Spalek, S. S. Saxena, C. Panagopoulos, T. Katsufuji, J. A. Schiemer, and M. A. Carpenter. *Elastic and Anelastic Relaxations Associated with Phase Transitions in $EuTiO_3$*. Phys. Rev. B **90**, 054119 (2014).

[184] V. Goian, S. Kamba, O. Pacherová, J. Drahokoupil, L. Palatinus, M. Dušek, J. Rohlíček, M. Savinov, F. Laufek, W. Schranz, A. Fuith, M. Kachlík, K. Maca, A. Shkabko, L. Sagarna, A. Weidenkaff, and A. A. Belik. *Antiferrodistortive Phase Transition in $EuTiO_3$*. Phys. Rev. B **86**, 054112 (2012).

[185] M. Allieta, M. Scavini, L. J. Spalek, V. Scagnoli, H. C. Walker, C. Panagopoulos, S. S. Saxena, T. Katsufuji, and C. Mazzoli. *Role of Intrinsic Disorder in the Structural Phase Transition of Magnetoelectric $EuTiO_3$*. Phys. Rev. B **85**, 184107 (2012).

[186] Z. Guguchia, Z. Salman, H. Keller, K. Roleder, J. Köhler, and A. Bussmann-Holder. *Complexity in the Structural and Magnetic Properties of Almost Multiferroic $EuTiO_3$*. Phys. Rev. B **94**, 220406 (2016).

[187] C. J. Fennie and K. M. Rabe. *Magnetic and Electric Phase Control in Epitaxial $EuTiO_3$ from First Principles*. Phys. Rev. Lett. **97**, 267602 (2006).

[188] P. J. Ryan, J.-W. Kim, T. Birol, P. Thompson, J.-H. Lee, X. Ke, P. S. Normile, E. Karapetrova, P. Schiffer, S. D. Brown, C. J. Fennie, and D. G. Schlom. *Reversible Control of Magnetic Interactions by Electric Field in a Single-Phase Material.* Nature Communications **4**, 1334 (2013).

[189] K. Kugimiya, K. Fujita, K. Tanaka, and K. Hirao. *Preparation and Magnetic Properties of Oxygen Deficient $EuTiO_{3-\delta}$ Thin Films.* Journal of Magnetism and Magnetic Materials **310**, Proceedings of the 17th International Conference on Magnetism, 2268 –2270 (2007).

[190] H. Akamatsu, K. Fujita, Y. Zong, N. Takemoto, S. Murai, and K. Tanaka. *Impact of Amorphization on the Magnetic Properties of EuO-TiO_2 system.* Phys. Rev. B **82**, 224403 (2010).

[191] D. Stornaiuolo, B. Jouault, E. Di Gennaro, A. Sambri, M. D'Antuono, D. Massarotti, F. M. Granozio, R. Di Capua, G. M. De Luca, G. P. Pepe, F. Tafuri, and M. Salluzzo. *Interplay between Spin-Orbit Coupling and Ferromagnetism in Magnetotransport Properties of a Spin-Polarized Oxide Two-Dimensional Electron System.* Phys. Rev. B **98**, 075409 (2018).

[192] T. Katsufuji and Y. Tokura. *Transport and Magnetic Properties of a Ferromagnetic Metal: $Eu_{1-x}R_xTiO_3$.* Phys. Rev. B **60**, R15021–R15023 (1999).

[193] K. Ahadi, Z. Gui, Z. Porter, J. W. Lynn, Z. Xu, S. D. Wilson, A. Janotti, and S. Stemmer. *Carrier Density Control of Magnetism and Berry Phases in Doped $EuTiO_3$.* APL Materials **6**, 056105 (2018).

[194] K. Ahadi, L. Galletti, and S. Stemmer. *Evidence of a Topological Hall Effect in $Eu_{1-x}Sm_xTiO_3$.* Applied Physics Letters **111**, 172403 (2017).

[195] G. Koster, B. L. Kropman, G. J. H. M. Rijnders, D. H. A. Blank, and H. Rogalla. *Quasi-Ideal Strontium Titanate Crystal Surfaces through Formation of Strontium Hydroxide.* Applied Physics Letters **73**, 2920–2922 (1998).

[196] M. Kawasaki, K. Takahashi, T. Maeda, R. Tsuchiya, M. Shinohara, O. Ishiyama, T. Yonezawa, M. Yoshimoto, and H. Koinuma. *Atomic Control of the $SrTiO_3$ Crystal Surface.* Science **266**, 1540–1542 (1994).

[197] D. H. Lowndes, D. B. Geohegan, A. A. Puretzky, D. P. Norton, and C. M. Rouleau. *Synthesis of Novel Thin-Film Materials by Pulsed Laser Deposition.* Science **273**, 898–903 (1996).

[198] P. R. Willmott and J. R. Huber. *Pulsed Laser Vaporization and Deposition.* Rev. Mod. Phys. **72**, 315–328 (2000).

[199] D. A. Glocker and S. Shah, eds. *Handbook of Thin Film Process Technology.* Vol. 1 (IOP Publishing, 2002).

[200] L. J. van der Pauw. *A Method of Measuring Specific Resistivity and Hall Effect of Discs of Arbitrary Shapes.* Philips Res. Repts. **13**, 1–9 (1958).

[201] L. J. van der Pauw. *A Method of Measuring the Resistivity and Hall Coefficient on Lamellae of Arbitrary Shape*. Philips Res. Repts. **20**, 220–224 (1958).

[202] Y. Wang, R. Ramaswamy, M. Motapothula, K. Narayanapillai, D. Zhu, J. Yu, T. Venkatesan, and H. Yang. *Room-Temperature Giant Charge-to-Spin Conversion at the $SrTiO_3-LaAlO_3$ Oxide Interface*. Nano Letters **17**, 7659–7664 (2017).

[203] D. Maryenko, A. S. Mishchenko, M. S. Bahramy, A. Ernst, J. Falson, Y. Kozuka, A. Tsukazaki, N. Nagaosa, and M. Kawasaki. *Observation of Anomalous Hall Effect in a Non-Magnetic Two-Dimensional Electron System*. Nature Communications **8**, 14777 (2017).

[204] P. Moetakef, T. A. Cain, D. G. Ouellette, J. Y. Zhang, D. O. Klenov, A. Janotti, C. G. Van de Walle, S. Rajan, S. J. Allen, and S. Stemmer. *Electrostatic Carrier Doping of $GdTiO_3/SrTiO_3$ Interfaces*. Applied Physics Letters **99**, 232116 (2011).

[205] M. N. Grisolia, J. Varignon, G. Sanchez-Santolino, A. Arora, S. Valencia, M. Varela, R. Abrudan, E. Weschke, E. Schierle, J. E. Rault, J.-P. Rueff, A. Barthélémy, J. Santamaria, and M. Bibes. *Hybridization-Controlled Charge Transfer and Induced Magnetism at Correlated Oxide Interfaces*. Nature Physics **12**, 484 (2016).

[206] T. Fix, F. Schoofs, J. L. MacManus-Driscoll, and M. G. Blamire. *Influence of Doping at the Nanoscale at $LaAlO_3/SrTiO_3$ Interfaces*. Applied Physics Letters **97**, 072110 (2010).

[207] S. Das, A. Rastogi, L. Wu, J.-C. Zheng, Z. Hossain, Y. Zhu, and R. C. Budhani. *Kondo Scattering in δ-doped $LaTiO_3/SrTiO_3$ Interfaces: Renormalization by Spin-Orbit Interactions*. Phys. Rev. B **90**, 081107 (2014).

[208] Y. C. Liao, T. Kopp, C. Richter, A. Rosch, and J. Mannhart. *Metal-Insulator Transition of the $LaAlO_3$-$SrTiO_3$ Interface Electron System*. Phys. Rev. B **83**, 075402 (2011).

[209] P. Reith, X. Renshaw Wang, and H. Hilgenkamp. *Analysing Magnetism Using Scanning SQUID Microscopy*. Review of Scientific Instruments **88**, 123706 (2017).

[210] B. Kalisky, J. A. Bert, B. B. Klopfer, C. Bell, H. K. Sato, M. Hosoda, Y. Hikita, H. Y. Hwang, and K. A. Moler. *Critical Thickness for Ferromagnetism in $LaAlO_3/SrTiO_3$ Heterostructures*. Nature Communications **3**, 922 (2012).

[211] B. Kalisky, J. A. Bert, C. Bell, Y. Xie, H. K. Sato, M. Hosoda, Y. Hikita, H. Y. Hwang, and K. A. Moler. *Scanning Probe Manipulation of Magnetism at the $LaAlO_3/SrTiO_3$ Heterointerface*. Nano Letters **12**, 4055–4059 (2012).

[212] J. Cumings, L. S. Moore, H. T. Chou, K. C. Ku, G. Xiang, S. A. Crooker, N. Samarth, and D. Goldhaber-Gordon. *Tunable Anomalous Hall Effect in a Nonferromagnetic System*. Phys. Rev. Lett. **96**, 196404 (2006).

[213] D. Culcer, A. Sekine, and A. H. MacDonald. *Interband Coherence Response to Electric Fields in Crystals: Berry-Phase Contributions and Disorder Effects*. Phys. Rev. B **96**, 035106 (2017).

[214] A. Fert and A. Friederich. *Skew Scattering by Rare-Earth Impurities in Silver, Gold, and Aluminum*. Phys. Rev. B **13**, 397–411 (1976).

[215] J. N. Chazalviel and I. Solomon. *Experimental Evidence of the Anomalous Hall Effect in a Nonmagnetic Semiconductor*. Phys. Rev. Lett. **29**, 1676–1679 (1972).

[216] S. R. Shinde, S. B. Ogale, J. S. Higgins, H. Zheng, A. J. Millis, V. N. Kulkarni, R. Ramesh, R. L. Greene, and T. Venkatesan. *Co-occurrence of Superparamagnetism and Anomalous Hall Effect in Highly Reduced Cobalt-Doped Rutile* $TiO_{2-\delta}$ *Films*. Phys. Rev. Lett. **92**, 166601 (2004).

[217] A. Yang, K. Zhang, S. Yan, S. Kang, Y. Qin, J. Pei, L. He, H. Li, Y. Dai, S. Xiao, and Y. Tian. *Superparamagnetism, Magnetoresistance and Anomalous Hall Effect in Amorphous* Mn_xSi_{1-x} *Semiconductor Films*. Journal of Alloys and Compounds **623**, 438 –441 (2015).

[218] S. X. Zhang, W. Yu, S. B. Ogale, S. R. Shinde, D. C. Kundaliya, W.-K. Tse, S. Y. Young, J. S. Higgins, L. G. Salamanca-Riba, M. Herrera, L. F. Fu, N. D. Browning, R. L. Greene, and T. Venkatesan. *Magnetism and Anomalous Hall Effect in* $Co-(La,Sr)TiO_3$. Phys. Rev. B **76**, 085323 (2007).

[219] S. Nakatsuji, N. Kiyohara, and T. Higo. *Large anomalous Hall effect in a non-collinear antiferromagnet at room temperature*. Nature **527**, 212 (2015).

[220] H. Chen, Q. Niu, and A. H. MacDonald. *Anomalous Hall Effect Arising from Noncollinear Antiferromagnetism*. Phys. Rev. Lett. **112**, 017205 (2014).

[221] P. Seiler, J. Zabaleta, R. Wanke, J. Mannhart, T. Kopp, and D. Braak. *Antilocalization at an Oxide Interface*. Phys. Rev. B **97**, 075136 (2018).

[222] N. Bovenzi and M. Diez. *Semiclassical Theory of Anisotropic Transport at* $LaAlO_3/SrTiO_3$ *Interfaces under an In-Plane Magnetic Field*. Phys. Rev. B **95**, 205430 (2017).

[223] M. Basletic, J.-L. Maurice, C. Carrétéro, G. Herranz, O. Copie, M. Bibes, É. Jacquet, K. Bouzehouane, S. Fusil, and A. Barthélémy. *Mapping the Spatial Distribution of Charge Carriers in* $LaAlO_3/SrTiO_3$ *Heterostructures*. Nature Materials **7**, 621 (2008).

[224] B. I. Edmondson, S. Liu, S. Lu, H. Wu, A. Posadas, D. J. Smith, X. P. A. Gao, A. A. Demkov, and J. G. Ekerdt. *Effect of $SrTiO_3$ Oxygen Vacancies on the Conductivity of $LaTiO_3$/$SrTiO_3$ Heterostructures.* Journal of Applied Physics **124**, 185303 (2018).

[225] S. W. Lee, Y. Liu, J. Heo, and R. G. Gordon. *Creation and Control of Two-Dimensional Electron Gas Using Al-Based Amorphous Oxides/$SrTiO_3$ Heterostructures Grown by Atomic Layer Deposition.* Nano Letters **12**, 4775–4783 (2012).

[226] D. Fuchs, R. Schäfer, A. Sleem, R. Schneider, R. Thelen, and H. von Löhneysen. *Two-Dimensional Superconductivity between $SrTiO_3$ and Amorphous Al_2O_3*. Applied Physics Letters **105**, 092602 (2014).

[227] P. Kumar, A. Dogra, and V. Toutam. *Pinhole Mediated Electrical Transport across $LaTiO_3$ / $SrTiO_3$ and $LaAlO_3$ / $SrTiO_3$ Oxide Hetero-structures.* Applied Physics Letters **103**, 211601 (2013).

[228] E. Flekser, M. Ben Shalom, M. Kim, C. Bell, Y. Hikita, H. Y. Hwang, and Y. Dagan. *Magnetotransport Effects in Polar Versus Non-polar $SrTiO_3$ Based Heterostructures.* Phys. Rev. B **86**, 121104 (2012).

[229] N. J. Goble, R. Akrobetu, H. Zaid, S. Sucharitakul, M.-H. Berger, A. Sehirlioglu, and X. P. A. Gao. *Anisotropic Electrical Resistance in Mesoscopic $LaAlO_3$ / $SrTiO_3$ Devices with Individual Domain Walls.* Scientific Reports **7**, 44361 (2017).

[230] R. Vaglio, C. Attanasio, L. Maritato, and A. Ruosi. *Explanation of the Resistance-Peak Anomaly in Nonhomogeneous Superconductors.* Phys. Rev. B **47**, 15302–15303 (1993).

[231] X. Wang, W. M. Lü, A. Annadi, Z. Q. Liu, K. Gopinadhan, S. Dhar, T. Venkatesan, and Ariando. *Magnetoresistance of Two-dimensional and Three-dimensional Electron Gas in $LaAlO_3$ / $SrTiO_3$ Heterostructures: Influence of Magnetic Ordering, Interface Scattering, and Dimensionality.* Phys. Rev. B **84**, 075312 (2011).

[232] M. M. Parish and P. B. Littlewood. *Non-saturating Magnetoresistance in Heavily Disordered Semiconductors.* Nature **426**, 162–165 (2003).

[233] T. Khouri, U. Zeitler, C. Reichl, W. Wegscheider, N. E. Hussey, S. Wiedmann, and J. C. Maan. *Linear Magnetoresistance in a Quasifree Two-Dimensional Electron Gas in an Ultrahigh Mobility GaAs Quantum Well.* Phys. Rev. Lett. **117**, 256601 (2016).

[234] J. Hu, M. M. Parish, and T. F. Rosenbaum. *Nonsaturating Magnetoresistance of Inhomogeneous Conductors: Comparison of Experiment and Simulation.* Phys. Rev. B **75**, 214203 (2007).

[235] F. Kisslinger, C. Ott, and H. B. Weber. *Origin of Nonsaturating Linear Magnetoresistivity*. Phys. Rev. B **95**, 024204 (2017).

[236] N. Ramakrishnan, Y. T. Lai, S. Lara, M. M. Parish, and S. Adam. *Equivalence of Effective Medium and Random Resistor Network Models for Disorder-Induced Unsaturating Linear Magnetoresistance*. Phys. Rev. B **96**, 224203 (2017).

[237] T. Schumann, M. Goyal, D. A. Kealhofer, and S. Stemmer. *Negative Magnetoresistance due to Conductivity Fluctuations in Films of the Topological Semimetal* Cd_3As_2. Phys. Rev. B **95**, 241113 (2017).

[238] J. Xu, M. K. Ma, M. Sultanov, Z.-L. Xiao, Y.-L. Wang, D. Jin, Y.-Y. Lyu, W. Zhang, L. N. Pfeiffer, K. W. West, K. W. Baldwin, M. Shayegan, and W.-K. Kwok. *Negative Longitudinal Magnetoresistance in Gallium Arsenide Quantum Wells*. Nature Communications **10**, 287 (2019).

[239] G. N. Daptary, S. Kumar, P. Kumar, A. Dogra, N. Mohanta, A. Taraphder, and A. Bid. *Correlated non-Gaussian Phase Fluctuations in* $LaAlO_3/SrTiO_3$ *Heterointerfaces*. Phys. Rev. B **94**, 085104 (2016).

[240] H. Thierschmann, E. Mulazimoglu, N. Manca, S. Goswami, T. M. Klapwijk, and A. D. Caviglia. *Transport Regimes of a Split Gate Superconducting Quantum Point Contact in the Two-Dimensional* $LaAlO_3/SrTiO_3$ *Superfluid*. Nature Communications **9**, 2276 (2018).

[241] S. Hurand, A. Jouan, E. Lesne, G. Singh, C. Feuillet-Palma, M. Bibes, A. Barthélémy, J. Lesueur, and N. Bergeal. *Josephson-like Dynamics of the Superconducting* $LaAlO_3/SrTiO_3$ *Interface*. Phys. Rev. B **99**, 104515 (2019).

[242] Y. Frenkel, N. Haham, Y. Shperber, C. Bell, Y. Xie, Z. Chen, Y. Hikita, H. Y. Hwang, E. K. H. Salje, and B. Kalisky. *Imaging and Tuning Polarity at* $SrTiO_3$ *Domain Walls*. Nature Materials **16**, 1203 (2017).

[243] Y.-Y. Pai, H. Lee, J.-W. Lee, A. Annadi, G. Cheng, S. Lu, M. Tomczyk, M. Huang, C.-B. Eom, P. Irvin, and J. Levy. *One-Dimensional Nature of Superconductivity at the* $LaAlO_3/SrTiO_3$ *Interface*. Phys. Rev. Lett. **120**, 147001 (2018).

[244] R. V. Vovk, G. Y. Khadzhai, I. L. Goulatis, S. N. Kamchatnaya, and A. Chroneos. *Diffusion of the Superconducting Transition in HTSC*. Journal of Materials Science: Materials in Electronics **28**, 10862–10865 (2017).

[245] H. S. Gamchi, G. J. Russell, and K. N. R. Taylor. *Resistive Transition for* $YBa_2Cu_3O_{7-\delta}$-Y_2BaCuO_5 *Composites: Influence of a Magnetic Field*. Phys. Rev. B **50**, 12950–12958 (1994).

[246] I. Felner, E. Galstyan, B. Lorenz, D. Cao, Y. S. Wang, Y. Y. Xue, and C. W. Chu. *Magnetoresistance Hysteresis and Critical Current Density in Granular* $RuSr_2Gd_{2-x}Ce_xCu_2O_{10-\delta}$. Phys. Rev. B **67**, 134506 (2003).

[247] M. Sandim and R. Jardim. *Intergranular Transport Properties of Polycrystalline* $Sm_{1.82}Ce_{0.18}CuO_{4-y}$ *under Low Applied Magnetic Fields*. Physica C: Superconductivity **328**, 246 –256 (1999).

[248] S. A. Wolf, D. U. Gubser, W. W. Fuller, J. C. Garland, and R. S. Newrock. *Two-Dimensional Phase Transition in Granular NbN Films*. Phys. Rev. Lett. **47**, 1071–1074 (1981).

[249] D. J. Resnick, J. C. Garland, J. T. Boyd, S. Shoemaker, and R. S. Newrock. *Kosterlitz-Thouless Transition in Proximity-Coupled Superconducting Arrays*. Phys. Rev. Lett. **47**, 1542–1545 (1981).

[250] D. W. Abraham, C. J. Lobb, M. Tinkham, and T. M. Klapwijk. *Resistive Transition in Two-Dimensional Arrays of Superconducting Weak Links*. Phys. Rev. B **26**, 5268–5271 (1982).

[251] Y. J. Qian, Z. M. Tang, K. Y. Chen, B. Zhou, J. W. Qiu, B. C. Miao, and Y. M. Cai. *Transport Hysteresis of the Oxide Superconductor* $Y_1Ba_2Cu_3O_{7-x}$ *in Applied Fields*. Phys. Rev. B **39**, 4701–4703 (1989).

[252] Y. V. Kopelevich, V. V. Lemanov, and V. V. Makarov. *Influence of Weak Bonds on Electrical Properties of* $YBa_2Cu_3O_{69}$ *Ceramics*. **32**, 3613–3617 (1990).

[253] K. Kwasnitza and C. Widmer. *Hysteretic Effects in the Flux-Flow State of Granular High-Tc Superconductors*. Physica C: Superconductivity **171**, 211 –215 (1990).

[254] C. dos Santos, M. da Luz, B. Ferreira, and A. Machado. *On the Transport Properties in Granular or Weakly Coupled Superconductors*. Physica C: Superconductivity **391**, 345 –349 (2003).

[255] P Muné, F. Fonseca, R Muccillo, and R. Jardim. *Magnetic Hysteresis of the Magnetoresistance and the Critical Current Density in Polycrystalline* $YBa_2Cu_3O_{7-\delta}$*–Ag Superconductors*. Physica C: Superconductivity **390**, 363 –373 (2003).

[256] D. A. Balaev, D. M. Gokhfeld, A. A. Dubrovskiĭ, S. I. Popkov, K. A. Shaikhutdinov, and M. I. Petrov. *Magnetoresistance Hysteresis in Granular HTSCs as a Manifestation of the Magnetic Flux Trapped by Superconducting Grains in YBCO + CuO Composites*. Journal of Experimental and Theoretical Physics **105**, 1174–1183 (2007).

[257] J. Evetts and B. Glowacki. *Relation of Critical Current Irreversibility to Trapped Flux and Microstructure in Polycrystalline* $YBa_2Cu_3O_7$. Cryogenics **28**, 641 –649 (1988).

[258] G. N. Daptary, S. Kumar, A. Bid, P. Kumar, A. Dogra, R. C. Budhani, D. Kumar, N. Mohanta, and A. Taraphder. *Observation of Transient Superconductivity at the $LaAlO_3/SrTiO_3$ Interface*. Phys. Rev. B **95**, 174502 (2017).

[259] M. E. McHenry, M. P. Maley, and J. O. Willis. *Systematics of Transport Critical-Current-Density Hysteresis in Polycrystalline Y-Ba-Cu-O*. Phys. Rev. B **40**, 2666–2669 (1989).

[260] L. Ji, M. S. Rzchowski, N. Anand, and M. Tinkham. *Magnetic-Field-Dependent Surface Resistance and Two-Level Critical-State Model for Granular Superconductors*. Phys. Rev. B **47**, 470–483 (1993).

[261] K. A. Delin, T. P. Orlando, E. J. McNiff, S. Foner, R. B. van Dover, L. F. Schneemeyer, and J. V. Waszczak. *High-Field Magnetization Scaling Relations for Pure and Ni-Substituted Single-Crystal $YBa_2Cu_3O_7$*. Phys. Rev. B **46**, 11092–11101 (1992).

[262] Půst, L. and Kadlecová, J. and Jirsa, M. and Durčok, S. *Correlation between Magnetic Hysteresis and Magnetic Relaxation in YBaCuO Single Crystals*. Journal of Low Temperature Physics **78**, 179–186 (1990).

[263] M Požek, I Ukrainczyk, B Rakvin, and A Dulčić. *Dynamic Measurements of Flux Creep and Flow in $YBa_2Cu_3O_{7-\delta}$ Single Crystals*. Europhysics Letters (EPL) **16**, 683–688 (1991).

[264] M. Jirsa, L. Pust, H. Schnack, and R. Griessen. *Extension of the Time Window for Investigation of Relaxation Effects in High-Tc Superconductors*. Physica C: Superconductivity **207**, 85 –96 (1993).

[265] G. Venditti, J. Biscaras, S. Hurand, N. Bergeal, J. Lesueur, A. Dogra, R. C. Budhani, M. Mondal, J. Jesudasan, P. Raychaudhuri, S. Caprara, and L. Benfatto. *Nonlinear $I-V$ Characteristics of Two-Dimensional Superconductors: Berezinskii-Kosterlitz-Thouless Physics versus Inhomogeneity*. Phys. Rev. B **100**, 064506 (2019).

[266] Y. Liu, D. B. Haviland, B. Nease, and A. M. Goldman. *Insulator-to-Superconductor Transition in Ultrathin Films*. Phys. Rev. B **47**, 5931–5946 (1993).

[267] B. Shklovskii and A. Efros. *Electronic Properties of Doped Semiconductors*. Springer Series in Solid-State Sciences (Springer Berlin Heidelberg, 1984).

[268] D. Mandrus, L. Forro, C. Kendziora, and L. Mihaly. *Two-dimensional Electron Localization in Bulk Single Crystals of $Bi_2Sr_2Y_xCa_{1-x}Cu_2O_8$*. Phys. Rev. B **44**, 2418–2421 (1991).

[269] D. B. Haviland, H. M. Jaeger, B. G. Orr, and A. M. Goldman. *Local Superconducting Coupling in the Strong-Localization Limit of Ultrathin Granular Metal Films*. Phys. Rev. B **40**, 719–722 (1989).

[270] C. G. L. Bøttcher, F. Nichele, M. Kjaergaard, H. J. Suominen, J. Shabani, C. J. Palmstrøm, and C. M. Marcus. *Superconducting, Insulating and Anomalous Metallic Regimes in a Gated Two-Dimensional Semiconductor-Superconductor Array*. Nature Physics **14**, 1138–1144 (2018).

[271] Z. Ye, I. F. Lyuksyutov, W. Wu, and D. G. Naugle. *Strongly Anisotropic Flux Pinning in Superconducting $Pb_{82}Bi_{18}$ Thin Films Covered by Periodic Ferromagnet Stripes*. Superconductor Science and Technology **24**, 024011 (2011).

[272] K. Tanaka, K. Fujita, Y. Maruyama, Y. Kususe, H. Murakami, H. Akamatsu, Y. Zong, and S. Murai. *Ferromagnetism Induced by Lattice Volume Expansion and Amorphization in $EuTiO_3$ Thin Films*. Journal of Materials Research **28**, 1031–1041 (2013).

[273] S. C. Chae, Y. J. Chang, D.-W. Kim, B. W. Lee, I. Choi, and C. U. Jung. *Magnetic Properties of Insulating $RTiO_3$ Thin Films*. Journal of Electroceramics **22**, 216–220 (2009).

[274] K. Hatabayashi, T. Hitosugi, Y. Hirose, X. Cheng, T. Shimada, and T. Hasegawa. *Fabrication of $EuTiO_3$ Epitaxial Thin Films by Pulsed Laser Deposition*. Japanese Journal of Applied Physics **48**, 100208 (2009).

[275] K. Jiang, R. Zhao, P. Zhang, Q. Deng, J. Zhang, W. Li, Z. Hu, H. Yang, and J. Chu. *Strain and Temperature Dependent Absorption Spectra Studies for Identifying the Phase Structure and Band Gap of $EuTiO_3$ Perovskite Films*. Phys. Chem. Chem. Phys. **17**, 31618–31623 (2015).

[276] F Trier, D. V. Christensen, and N Pryds. *Electron Mobility in Oxide Heterostructures*. Journal of Physics D: Applied Physics **51**, 293002 (2018).

[277] E. Mikheev, B. Himmetoglu, A. P. Kajdos, P. Moetakef, T. A. Cain, C. G. Van de Walle, and S. Stemmer. *Limitations to the room Temperature Mobility of Two- and Three-Dimensional Electron Liquids in $SrTiO_3$*. Applied Physics Letters **106**, 062102 (2015).

[278] A. Fête, S. Gariglio, A. D. Caviglia, J.-M. Triscone, and M. Gabay. *Rashba Induced Magnetoconductance Oscillations in the $LaAlO_3$-$SrTiO_3$ Heterostructure*. Phys. Rev. B **86**, 201105 (2012).

[279] K. Bethe. *Über Das Mikrowellenverhalten Nichtlinearer Dielektrika*. Philips Res. Repts Suppl. **№ 2** (1970).

[280] O. G. Vendik, E. K. Hollmann, A. B. Kozyrev, and A. M. Prudan. *Ferroelectric Tuning of Planar and Bulk Microwave Devices*. Journal of Superconductivity **12**, 325–338 (1999).

[281] R. C. Neville, B. Hoeneisen, and C. A. Mead. *Permittivity of Strontium Titanate*. Journal of Applied Physics **43**, 2124–2131 (1972).